Struct Multidisc Optim (2017) 55:2045–2072
DOI 10.1007/s00158-016-1627-7

RESEARCH PAPER

Material nonlinear topology optimization using the ground structure method with a discrete filtering scheme

Xiaojia Zhang[1] · **Adeildo S. Ramos Jr.**[2] · **Glaucio H. Paulino**[1]

Received: 3 June 2016 / Revised: 13 November 2016 / Accepted: 18 November 2016 / Published online: 3 March 2017

Abstract Topology optimization of truss lattices, using the ground structure method, is a practical engineering tool that allows for improved structural designs. However, in general, the final topology consists of a large number of undesirable thin bars that may add artificial stiffness and degenerate the condition of the system of equations, sometimes even leading to an invalid structural system. Moreover, most work in this field has been restricted to linear material behavior, yet real materials generally display nonlinear behavior. To address these issues, we present an efficient filtering scheme, with reduced-order modeling, and demonstrate its application to two- and three-dimensional topology optimization of truss networks considering multiple load cases and nonlinear constitutive behavior. The proposed scheme accounts for proper load levels during the optimization process, yielding the displacement field without artificial stiffness by simply using the truss members that actually exist in the structure (spurious members are removed), and improving convergence performance. The nonlinear solution scheme is based on a Newton-Raphson approach with line search, which is essential for convergence. In addition, the use of reduced-order information significantly reduces the size of the structural and optimization problems within a few iterations, leading to drastically improved computational performance. For instance, the application of our method to a problem with approximately 1 million design variables shows that the proposed filter algorithm, while offering almost the same optimized structure, is more than 40 times faster than the standard ground structure method.

Keywords Ground structure method · Filter · Hyperelastic trusses · Topology optimization · Potential energy · Tikhonov regularization · Newton-Raphson · Line search

Dedicated to the memory of Professor George I. N. Rozvany (August 27, 1930–July 31, 2015)

✉ Glaucio H. Paulino
paulino@gatech.edu

Xiaojia Zhang
xzhang645@gatech.edu

Adeildo S. Ramos Jr.
adramos@lccv.ufal.br

[1] School of Civil and Environmental Engineering, Georgia Institute of Technology, 790 Atlantic Drive, Atlanta, GA, 30332, USA

[2] Laboratory of Scientific Computing and Visualization Technology Center, Federal University of Alagoas, Maceió, AL, 57092–970, Brazil

1 Introduction

Truss lattice networks can be optimized using the ground structure method (GSM) (see, e.g., Dorn et al. 1964; Kirsch 1989; Rozvany et al. 1995; Bendsøe and Sigmund 2003; Christensen and Klarbring 2009). In the field of structural topology optimization of trusses using the GSM, it is important to take into account material nonlinearity, because real materials generally display nonlinear constitutive relationship. Topology optimization considering linear material behavior (the prevailing approach in the literature (Bendsøe and Sigmund 2003)) has a limited scope, which can be extended by accounting for nonlinear material as it can significantly alter the optimized structure layout. In fact, the studies of material nonlinearity using the GSM (e.g., Achtziger 1996; Ohsaki 2010; Sokół 2011; Ramos Jr and Paulino 2015) show the importance

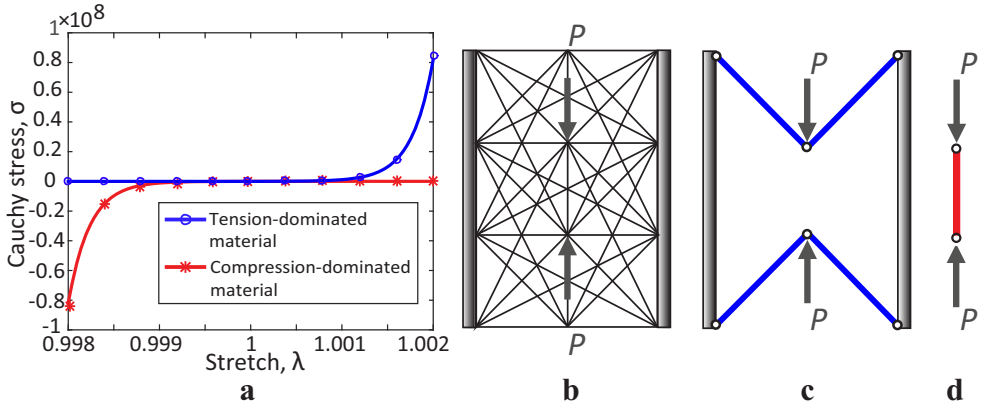

Fig. 1 Influence of material properties in topology optimization: **a** Hyperelastic Ogden-based material models with convex[1] specific strain energy; **b** initial ground structure and boundary conditions; **c** final filtered topology from the tension-dominated Ogden-based material model; **d** either linear elastic material or the compression-dominated Ogden-based material model yields a self-equilibrated filtered topology. Blue bars are in tension and the red bar is in compression (online version in color)

of accounting for nonlinear material properties and load levels in structural optimization. Figure 1 further illustrates and motivates the influence of material nonlinearity in optimization. Two hyperelastic material models with convex specific strain energy, representing tension-dominated and compression-dominated Ogden-based materials, lead to completely different final topologies. In addition, the self-equilibrated filtered structure in Fig. 1d (from the compression-dominated material) is a motivation for solving systems with a singular stiffness matrix (Ramos Jr and Paulino 2016).

1.1 Structural engineering perspective

From the perspective of structural engineering, one limitation of the standard GSM is its inability to define a valid final structure and the unlikelihood of manufacturing an optimized structure. Because a cut-off value is needed to define the final topology for the standard GSM (a sizing problem), the topology may either consist of a large number of undesirable thin bars (if the cut-off value is too small) or violate the global equilibrium (if the cut-off value is too large) because of the removal of some structurally important bars. This is illustrated by means of Fig. 2, which shows a bridge (Fig. 2a) with a bilinear material model (Fig. 2b). For comparison purposes, Fig. 2c shows the case when a proper cut-off is chosen and Fig. 2d shows the case when global equilibrium is violated because of an improper choice of the final cut-off value, both of them using the same lower bound on the design variable, $x_{\min} = 1.36 \times 10^{-8}$. Figure 2e and f illustrate the final topologies without a cut-off value. Figure 2e is obtained using the standard GSM with an arbitrarily small lower bound of the design variable, $x_{\min} = 1.36 \times 10^{-14}$. As a result, the entire ground structure is included in the final topology. Figure 2f shows the final topology with $x_{\min} = 0$ as the lower bound, in which the final topology consists of numerous thin bars. Note that the zero lower bound on design variables leads to singular tangent stiffness matrices. In this case, state equations were solved by minimization of potential energy with Tikhonov regularization (Ramos Jr and Paulino 2016). For other methods of solving the state equations, readers are referred to Bruns (2006), Washizawa et al. (2004), and Wang et al. (2007). Attempts have been made to treat undesirable thin members and obtain valid and constructible structures. By introducing discrete variables (either as design variables or as the existence variable) into the optimization, the undesirable thin bars may be avoided. For example, Tangaramvong et al. (2014) impose a realistic design constraint with a binary variable (to represent presence or absence) on the braces with geometric nonlinearity, which only selects braces within specific bound limits. However, these formulations with discrete variables to treat thin members become mixed integer linear/nonlinear problems. For a detailed review of the truss optimization with discrete design variables, readers are referred to Stolpe (2016). Another approach consists of including "slenderness constraints" using a plastic formulation - see Achtziger (1999a, b). Here we adopt an elastic formulation as motivated by a recent study by Ramos Jr and Paulino (2016),

[1]The tension-dominated material has $(\beta_1, \beta_2) = (4264.0, -0.9)$ and the compression-dominated material has $(\beta_1, \beta_2) = (1.1, -4253.4)$, where β_1 and β_2 are material parameters for Ogden-based material models – see Section 3.1 for the constitutive model definition.

who propose a discrete filter that can be used to control the final resolution of the optimized structure, resulting in a valid structure in which global equilibrium is guaranteed. This discrete filter has only been applied to linear optimization problems; therefore, in an effort to provide a practical design tool that targets the real-life demands of material, structural design, and manufacturing aspects, we propose a filtering scheme with reduced-order modeling that accounts for material nonlinearity in this paper.

1.2 Analysis perspective

From an analysis perspective, the standard GSM considering material nonlinearity, contains numerous small area truss members, which can be problematic in two aspects: first, because small area members are included in the solution of the structural problem, they add artificial stiffness to the structure, leading to a degree of unreliability of the optimization results. Moreover, in the nonlinear finite element method (FEM) of the standard GSM, certain nodes that only connect to thin members produce small eigenvalues in the stiffness matrix, which could degenerate the condition of the state equations and result in difficulties in convergence. Nevertheless, the removal of these thin members can result in a violation of global equilibrium, as shown in Fig. 2d. The proposed filter algorithm, however, filters out the small area members and the associated nodes in the structure thus solving such structural problems (state equations) solely by using other relevant members. As a result, the displacement field is obtained, which improves the convergence performance in the nonlinear FEM and allows global equilibrium verification in the actual topology.

1.3 Efficiency perspective

From the perspective of efficiency, another major problem with the GSM that accounts for material nonlinearity is the high computational cost of the iterative procedure for solving nonlinear structural systems. Furthermore, the incorporation of the multiple load cases into the nonlinear problems leads to higher computational cost, because each load case requires an independent iterative nonlinear FE analysis. To minimize the cost, a fully reduced-order model is used in the filtering scheme, which solves both the state and optimization problems of the filtered structures. As a result of the smaller sizes of the tangent stiffness matrix and the sensitivity vector, the use of the proposed filtering scheme with the fully reduced-order model significantly improves the computational performance of the optimization algorithm.

1.4 Paper context and content

This work is based on an elastic formulation with the total potential energy used in both the objective function and the structural problem[2] (see, e.g., Stricklin and Haisler 1977; Haftka and Kamat 1989; Toklu 2004; Hassani and Hinton 1998; Khot and Kamat 1985; Klarbring and Strömberg 2012, 2013; Ramos Jr and Paulino 2015). Other types of objective functions in nonlinear problems have been studied by other authors (see, e.g., Buhl et al. 2000; Kemmler et al. 2005; Sekimoto and Noguchi 2001).

The remainder of the paper is organized as follows. Section 2 presents the standard, modified standard, and filter formulations adopted for the nonlinear optimization problem under multiple load cases, followed by sensitivity analysis, convexity proof, and KKT conditions. Section 3 describes the truss models with material nonlinearity, corresponding potential energy, linearization of the governing equations, and the methods of solving the state equations. Section 4 introduces the reduced-order model in the state and the optimization problems. Section 5 presents numerical examples in two- and three-dimensions highlighting the properties of the proposed method, and Section 6 provides concluding remarks with suggestions for extending the work.

2 Nested optimization formulations for nonlinear problems considering multiple load cases

In this section, we examine the standard and the modified standard nested formulations as well as the filter formulation of the nonlinear optimization problem considering multiple load cases. In addition, the sensitivity analysis, convexity proof, a conceptual example with unbounded solution, and the KKT conditions are presented.

2.1 Standard and modified standard formulations (without filter)

First, we present the *standard nested formulation* and the solution algorithm of topology optimization for trusses with nonlinear constitutive models and small deformation. The topology design consists of determining the cross-sectional areas of the truss elements using the ground structure (GS) approach. By definition, the standard total potential energy

[2] In general, it can be seen as a surrogate for understanding the field of nonlinear topology optimization.

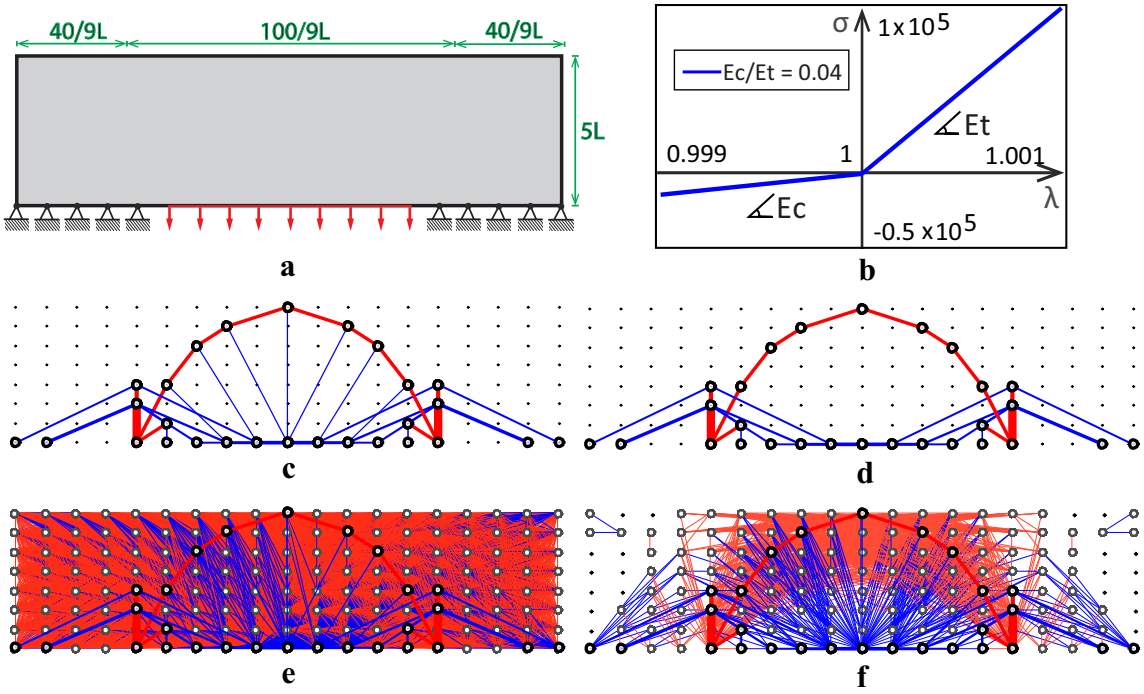

Fig. 2 Some pitfalls of the standard GSM through a case study of a bridge design with a full-level standard GS containing 7,083 non-overlapping members: **a** Bridge domain and boundary conditions; **b** bilinear material model with $E_c/E_t = 0.04$; **c** final topology (41 members) considering a lower bound on area, $x_{\min} = 1.36 \times 10^{-8}$, with a proper cut-off value which shows that global equilibrium holds; **d** final topology (34 members) considering a lower bound on area, $x_{\min} = 1.36 \times 10^{-8}$, with an improper cut-off value which shows that global equilibrium does not hold; **e** final topology (7,083 members) without the cut-off value considering a relatively small lower bound on area, $x_{\min} = 1.36 \times 10^{-14}$(standard GSM formulation); **f** final topology (975 members with non-zero area) without the cut-off value considering zero lower bound on area, $x_{\min} = 0$ (modified GSM with Tikhonov regularization). *Blue bars* are in tension and *red bars* are in compression (online version in color)

of the structure is $\Pi(\boldsymbol{u}) = U(\boldsymbol{u}) + \Omega(\boldsymbol{u})$, where $\boldsymbol{u}$ is the displacement vector, $U(\boldsymbol{u})$ is the strain energy, and $\Omega(\boldsymbol{u})$ is the total potential of the loads, given by

$$\begin{aligned} U(\boldsymbol{u}) &= \sum_{i=1}^{n} \int_{V^{(i)}} \Psi^{(i)}(\boldsymbol{u}) \, \mathrm{d}V \\ &= \sum_{i=1}^{n} V^{(i)} \Psi^{(i)}(\boldsymbol{u}) \\ &= \sum_{i=1}^{n} x^{(i)} L^{(i)} \Psi^{(i)}(\boldsymbol{u}), \end{aligned} \tag{1}$$

and

$$\Omega(\boldsymbol{u}) = -\boldsymbol{F}^{\mathrm{T}} \boldsymbol{u}, \tag{2}$$

where $\Psi^{(i)}(\boldsymbol{u})$, $x^{(i)}$, $L^{(i)}$, and $V^{(i)}$ are the specified strain energy function, the cross-sectional area, the length, and the volume of truss member i, respectively. The specified strain energy function, $\Psi^{(i)}(\boldsymbol{u})$, is assumed to be convex and differentiable for any given $\boldsymbol{u}$. The parameter n denotes the total number of truss members and $\boldsymbol{F}$ is the external load vector. We use the following nested formulation for the optimization problem under m load cases:

$$\begin{aligned} \min_{\boldsymbol{x}} \; & J(\boldsymbol{x}) = \min_{\boldsymbol{x}} \sum_{j=1}^{m} -w_j \Pi_j \left(\boldsymbol{x}, \boldsymbol{u}_j(\boldsymbol{x})\right) \\ \text{s.t. } & g(\boldsymbol{x}) = \boldsymbol{L}^{\mathrm{T}} \boldsymbol{x} - V_{\max} \le 0 \\ & 0 < x_{\min}^{(i)} \le x^{(i)} \le x_{\max}^{(i)}, \; i = 1, \ldots, n \\ \text{with } & \boldsymbol{u}_j(\boldsymbol{x}) = \arg\min_{\boldsymbol{u}} \Pi_j(\boldsymbol{x}, \boldsymbol{u}), \; j = 1, \ldots, m, \end{aligned} \tag{3}$$

where the objective function[3] $J(\boldsymbol{x}) = \sum_{j=1}^{m} -w_j \Pi_j(\boldsymbol{x}, \boldsymbol{u}_j(\boldsymbol{x}))$ is the additive inverse of a weighted sum of the total potential energy of the system in equilibrium state from each load case (Ramos Jr and Paulino 2015), where Π_j is the total potential energy of the equilibrated system under the jth load $\boldsymbol{F}_j$, w_j is the corresponding weight (strictly positive), $\boldsymbol{u}_j$ is the equilibrating displacement field (state variable) under load case $\boldsymbol{F}_j$, $\boldsymbol{x}$ and $\boldsymbol{L}$ are the vectors of

[3] In order to provide a physical explanation for the objective function, notice that when the prescribed displacements is zero on the boundary S_u, $J = U_c$ where S_u is the portion of the boundary where displacement boundary condition is applied and U_c is the complementary energy at the equilibrium configuration (see Ramos Jr and Paulino (2015)).

cross-sectional area (design variable) and length of truss members, respectively, $V_{\max}$ is the maximum material volume, and $x_{\min}^{(i)}$ and $x_{\max}^{(i)}$ denote the positive lower and upper bounds of the design variable of member i, respectively. The objective function is based on the min-max formulation described in Klarbring and Ströberg (2012, 2013). Following common practice (Christensen and Klarbring 2009), in this standard approach, we introduce the strictly positive lower bound $x_{\min}^{(i)}$ to prevent the singular tangent stiffness matrix from forming (Christensen and Klarbring 2009). As a result, this standard nested formulation in (3) is a sizing problem. At the end of the optimization scheme, we use a "cut-off" approach for design variables to define the final topology. In this paper, we assume that the specific strain energy is a convex function and the structural model can carry each load case $\boldsymbol{F}_j$, $j = 1, ..., m$, (i.e., the equilibrium condition is satisfied, $\boldsymbol{T}\left(\boldsymbol{x}, \boldsymbol{u}_j\right) = \boldsymbol{F}_j$, $j = 1, ..., m$). For the standard formulation (3), these assumptions, with the strictly positive lower bound on design variables, lead to the convexity of the potential energy with respect to the displacement field $\boldsymbol{u}$ (strict convexity of the potential energy requires the strictly convex specific strain energy and $x_{\min}^{(i)} > 0$), which ensures the attainability of a finite solution, $\boldsymbol{u}_j$, for each load case $\boldsymbol{F}_j$ in the structural model for any fixed feasible $\boldsymbol{x}$.

For the *modified standard optimization formulation* for trusses with material nonlinearity, we relax the lower bound of the design variables and require $x^{(i)} \geq 0$ for $i = 1, ..., n$. The formulation then becomes,

$$\begin{aligned} \min_{\boldsymbol{x}} \; J\left(\boldsymbol{x}\right) &= \min_{\boldsymbol{x}} \sum_{j=1}^{m} -w_j \Pi_j \left(\boldsymbol{x}, \boldsymbol{u}_j\left(\boldsymbol{x}\right)\right) \\ \text{s.t. } g\left(\boldsymbol{x}\right) &= \boldsymbol{L}^{\mathrm{T}}\boldsymbol{x} - V_{\max} \leq 0 \\ 0 \leq x^{(i)} &\leq x_{\max}^{(i)},\; i = 1, ..., n \\ \text{with } \boldsymbol{u}_j\left(\boldsymbol{x}\right) &= \arg\min_{\boldsymbol{u}} \left[\Pi_j\left(\boldsymbol{x}, \boldsymbol{u}\right) + \frac{\eta_j}{2}\boldsymbol{u}^{\mathrm{T}}\boldsymbol{u}\right],\; j = 1, ..., m. \end{aligned} \tag{4}$$

In the modified standard formulation, the lower bound of the design variables becomes the value of zero, showing that truss members can be removed by the update scheme from the problem (Ramos Jr and Paulino 2016). This modification on the lower bound of design variables transforms the sizing problem in (3) into a topology optimization problem. In addition, to prevent the possibility of a singular tangent stiffness matrix from forming in the Newton-Raphson method for the structural nonlinear equations, we introduce a Tikhonov regularization term (Tikhonov and Arsenin 1977; Felippa n.d; Ramos Jr and Paulino 2016; Talischi and Paulino 2013), $\frac{\eta_j}{2}\boldsymbol{u}^{\mathrm{T}}\boldsymbol{u}$, for jth load case, where η_j is the regularization parameter. The details of the Tikhonov regularization on the potential energy are shown in Section 3.4. For the modified standard formulation in (4), because we assume that specific strain energy is a convex function and the structural model can carry each load case $\boldsymbol{F}_j$, $j = 1, ..., m$, (i.e., the equilibrium condition is satisfied, $\boldsymbol{T}\left(\boldsymbol{x}, \boldsymbol{u}_j\right) = \boldsymbol{F}_j$, $j = 1, ..., m$), the potential energy is a convex function with respect to the displacement field $\boldsymbol{u}$ and the obtained $\boldsymbol{u}_j$ is a global minimum. By further including the Tikhonov regularization in the potential energy in the structural problem, the potential energy becomes strictly convex with respect to $\boldsymbol{u}$, in this case, the global minimum $\boldsymbol{u}_j$ for load case j is unique.

2.2 Filter formulation

Here, denoting α_f as the filter parameter for controlling the resolution of the topology, we introduce the filter operation as follows:

$$\mathit{Filter}\left(\boldsymbol{x}, \alpha_f, i\right) = \begin{cases} 0, & \text{if } \frac{x^{(i)}}{\max(\boldsymbol{x})} < \alpha_f < 1, \\ x^{(i)}, & \text{otherwise.} \end{cases} \tag{5}$$

We perform the filter operation every N_f steps during the optimization process to remove the information associated with the set of truss members with normalized areas below the filter parameter α_f, where N_f is prescribed by the user to determine how frequently to perform the filter operation. We denote $x_f^{(i)}$ as the filtered cross-sectional area associated with truss member i. In order to compare the final resolution of the results, we define the resolution of the filtered structure, α_{Top}, as follows,

$$\alpha_{\text{Top}} = \frac{\min\left(\boldsymbol{x}_f\right)}{\max\left(\boldsymbol{x}_f\right)}. \tag{6}$$

Figure 3 illustrates the filtering scheme. With the filter operation above, we introduce the filter formulation for optimization of trusses with material nonlinearity as follows:

$$\begin{aligned} \min_{\boldsymbol{x}} \; J\left(\boldsymbol{x}\right) &= \min_{\boldsymbol{x}} \sum_{j=1}^{m} -w_j \Pi_j \left(\boldsymbol{x}_f\left(\boldsymbol{x}\right), \boldsymbol{u}_j\left(\boldsymbol{x}\right)\right) \\ \text{s.t. } g\left(\boldsymbol{x}\right) &= \boldsymbol{L}^{\mathrm{T}}\boldsymbol{x}_f\left(\boldsymbol{x}\right) - V_{\max} \leq 0 \\ 0 \leq x^{(i)} &\leq x_{\max}^{(i)},\; i = 1, ..., n \\ \text{with } \boldsymbol{u}_j\left(\boldsymbol{x}\right) &= \arg\min_{\boldsymbol{u}} \left[\Pi_j\left(\boldsymbol{x}_f\left(\boldsymbol{x}\right), \boldsymbol{u}\right) + \frac{\eta_j}{2}\boldsymbol{u}^{\mathrm{T}}\boldsymbol{u}\right],\; j = 1, ..., m \\ \text{and } x_f^{(i)} &= \mathit{Filter}\left(\boldsymbol{x}, \alpha_f, i\right),\; i = 1, ..., n. \end{aligned} \tag{7}$$

where the subscript f denotes a filtered value. Algorithm 1 shows the implementation of our proposed algorithm. We note that this is a simplified procedure aiming at relatively low values of the filter α_f. For a more detailed discussion of the filter, see Ramos Jr and Paulino (2016).

2.3 Sensitivity analysis

In this paper, we perform sensitivity analysis in the filtered structure, i.e. by means of a reduced-order model in the

Algorithm 1 Optimization with the discrete filter

Initialize: $\boldsymbol{x}^0$, α_f, $\text{iter}_{\max}$, tol_{opt}, tol_{obj}, tol_{eqm}
for $k = 0, 1, ..., \text{iter}_{\max}$ **do**
  Filter: $x_f^{(i),k} = Filter\left(\boldsymbol{x}^k, \alpha_f, i\right),\ i = 1, ..., n.$
  for $j = 1, 2, ..., m$ **do**
    Solve: $\boldsymbol{u}_j\left(\boldsymbol{x}^k\right) = \arg\min_{\boldsymbol{u}} \left[\Pi_j\left(\boldsymbol{x}_f^k\left(\boldsymbol{x}^k\right), \boldsymbol{u}\right) + \frac{\eta_j}{2}\boldsymbol{u}^{\mathrm{T}}\boldsymbol{u}\right]$
  end for
  Compute: $J\left(\boldsymbol{x}^k\right)$, $g\left(\boldsymbol{x}^k\right)$, $\partial J\left(\boldsymbol{x}^k\right)/\partial x^{(i)}$, and $\partial g\left(\boldsymbol{x}^k\right)/\partial x^{(i)}$ using (7), (9), and (10)
  if $J\left(\boldsymbol{x}^k\right) - J\left(\boldsymbol{x}^{k-1}\right) > \text{tol}_{\text{obj}}$ or $||\boldsymbol{R}_{\text{Top}}^k||/||\boldsymbol{F}_{\text{Top}}|| > \text{tol}_{\text{eqm}}$ **then**
    quit
  end if
  Update: $\boldsymbol{x}^{k+1}$ using Optimality Criteria
  if $||\boldsymbol{x}^{k+1} - \boldsymbol{x}^k||_\infty < \text{tol}_{\text{opt}}$ **then**
    quit **for**
  end if
end for
$\boldsymbol{x}^{\text{final}} = \boldsymbol{x}^{k+1}$
End-filter: $x_f^{(i),\text{final}} = Filter\left(\boldsymbol{x}^{\text{final}}, \alpha_f, i\right),\ i = 1, ..., n.$
Solve: $\boldsymbol{u}_j\left(\boldsymbol{x}^{\text{final}}\right), j = 1, ..., m.$
if $||\boldsymbol{R}_{\text{Top}}^{\text{final}}||/||\boldsymbol{F}_{\text{Top}}|| > \text{tol}_{\text{eqm}}$ **then**
  quit
end if
Compute: $J\left(\boldsymbol{x}^{\text{final}}\right)$
Remove aligned nodes
Plot final topology

optimization problem, which indicates that the dimension of the sensitivity vector is the same as that of the filtered design variables. Under the assumption of global equilibrium, and since $\boldsymbol{u}_j$ is the equilibrating displacement field under load case $\boldsymbol{F}_j$, then the sensitivity of the objective function is given by,

$$\frac{\partial J(\boldsymbol{x})}{\partial x^{(i)}} = -\sum_{j=1}^{m} w_j \frac{\partial \Pi_j}{\partial x^{(i)}}\left(\boldsymbol{x}, \boldsymbol{u}_j(\boldsymbol{x})\right). \tag{8}$$

The external work in (2) for each load case is (explicitly) independent of the design variables. By using (1), we obtain the sensitivity as,

$$\begin{aligned}\frac{\partial J(\boldsymbol{x})}{\partial x^{(i)}} &= -\sum_{j=1}^{m} w_j \frac{\partial \Pi_j}{\partial x^{(i)}}\left(\boldsymbol{x}, \boldsymbol{u}_j(\boldsymbol{x})\right) \\ &= -\sum_{j=1}^{m} w_j \frac{\partial\left[\sum_{k=1}^{n} x^{(k)} L^{(k)} \Psi^{(k)}\left(\boldsymbol{u}_j(\boldsymbol{x})\right)\right]}{\partial x^{(i)}} \\ &= -\sum_{j=1}^{m} w_j L^{(i)} \Psi^{(i)}\left(\boldsymbol{u}_j(\boldsymbol{x})\right).\end{aligned} \tag{9}$$

Note that the sensitivity given by (9) is always non-positive because $L^{(i)}\Psi^{(i)}\left(\boldsymbol{u}_j(x)\right) \geq 0, j = 1, ..., m$. The sensitivity of the volume constraint for member i is calculated as

$$\frac{\partial g(\boldsymbol{x})}{\partial x^{(i)}} = L^{(i)}. \tag{10}$$

2.4 Convexity proof

In this subsection, we investigate the convexity condition of the modified standard topology optimization formulation in (4), i.e. the optimization formulation considering multiple load cases with hyperelastic nonlinear materials with convex specific strain energy and design variables $\boldsymbol{x} \geq \boldsymbol{0}$. Note that the standard nested formulation with linear structural model and end-compliance objective function has been proved to be convex by Svanberg (1984) for positive definite stiffness matrix, and by Achtziger (1997) for positive semi-definite stiffness matrix. The standard formulation in (3) with hyperelastic truss model and the objective function of total potential energy under single load case has been proved to be convex by Ramos Jr and Paulino (2015)

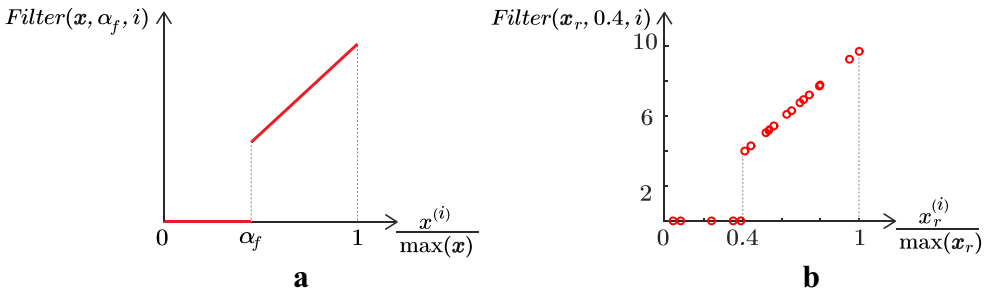

Fig. 3 Illustration of the filter operator: **a** theoretical and **b** numerical, displaying the output of a function with $\alpha_f = 0.4$ and a given random vector $\boldsymbol{x}_r$ for $i = 1, ..., 20$.[6] The function, implemented in Matlab, is provided in Appendix A

for positive definite tangent stiffness matrix. Since the constraint function, $\boldsymbol{L}^{\mathrm{T}}\boldsymbol{x} - V_{\max} \leq 0$ is convex, we need to study the convexity of the objective function,

$$\begin{aligned} J(\boldsymbol{x}) &= -\sum_{j=1}^{m} w_j \min_{\boldsymbol{u}} \Pi_j(\boldsymbol{x}, \boldsymbol{u}) \\ &= \sum_{j=1}^{m} w_j \max_{\boldsymbol{u}} \left[-\Pi_j(\boldsymbol{x}, \boldsymbol{u})\right] \\ &= \sum_{j=1}^{m} w_j \max_{\boldsymbol{u}} \left\{\boldsymbol{F}_j^{\mathrm{T}}\boldsymbol{u} - U(\boldsymbol{x}, \boldsymbol{u})\right\} \\ &= \sum_{j=1}^{m} w_j J_j(\boldsymbol{x}), \end{aligned} \tag{11}$$

to prove the convexity of the optimization formulation. Assuming that the strain energy is a convex function[4] and the structural model can carry each load case $\boldsymbol{F}_j$, $j = 1, ..., m$, (the equilibrium condition is satisfied, i.e., $\boldsymbol{T}(\boldsymbol{x}, \boldsymbol{u}_j) = \boldsymbol{F}_j$, $j = 1, ..., m$), we then have a finite solution, i.e. $\boldsymbol{u}_j(\boldsymbol{x})$, for each load case $\boldsymbol{F}_j$ in the structural model for a fixed $\boldsymbol{x}$. Under these conditions, since the strain energy $U(\boldsymbol{x}, \boldsymbol{u}) = \sum_{i=1}^{n} x^{(i)} L^{(i)} \Psi^{(i)}(\boldsymbol{u})$ is a linear function in $\boldsymbol{x}$ for a fixed $\boldsymbol{u}$, then $J_j(\boldsymbol{x})$ is a pointwise supremum function of a set of linear functions in $\boldsymbol{x}$,

$$J_j(\boldsymbol{x}) = \sup_{\boldsymbol{u}} \left\{ J_{j,\boldsymbol{u}}(\boldsymbol{x}) \,|\boldsymbol{u} \in \mathbb{R}^N \right\}, \tag{12}$$

where $J_{j,\boldsymbol{u}}(\boldsymbol{x}) = \boldsymbol{F}_j^{\mathrm{T}}\boldsymbol{u} - \sum_{i=1}^{n} x^{(i)} L^{(i)} \Psi^{(i)}(\boldsymbol{u})$ is convex, and N denotes the number of degrees of freedom (DOFs). We know that a function defined as the pointwise supremum of a set of convex functions is convex (Rockafellar 1970) and the weighted sum (with strictly positive weights) of convex functions is still convex. Therefore, $J(\boldsymbol{x})$ is convex under the assumptions that specific strain energy of the structural model is convex and the equilibrium condition is satisfied (see Achtziger 1997; Stolpe and Svanberg 2001 for proofs in the linear case under single load case). This proof is valid even when the tangent stiffness matrix is positive semidefinite, i.e., $\boldsymbol{x} \geq \boldsymbol{0}$ for the design variables and $\mathrm{d}\sigma(\lambda)/\mathrm{d}\lambda \geq 0$ for the nonlinear structural model (no requirement on the strict convexity), generalizing the convexity proof of Ramos Jr and Paulino (2015) for positive definite tangent stiffness matrix.

2.5 Conceptual example: unbounded solution

Figure 4 illustrates the case with unbounded solution because the structural model cannot carry the load, i.e., the equilibrium condition cannot be satisfied: $\boldsymbol{T}(\boldsymbol{x}, \boldsymbol{u}(\boldsymbol{x})) \neq \boldsymbol{F}$, with the bilinear model 1 (compression is not allowed in this material). Although the specific strain energy of this material model is convex, this case results in $J(\boldsymbol{x}) \to +\infty$ and leads to unbounded solution (Achtziger 1997), as shown in Fig. 4c.[5] The compression-dominated bilinear model 2 leads to a self-equilibrated structure in Fig. 4d. Note that the specific strain energy of these material models (Fig. 4a) is convex (not strictly convex). For the modified formulation (4), the potential energy with these material models and Tikhonov regularization becomes strictly convex. For the standard formulation (3), the potential energy with these material models is convex (not strictly convex).

2.6 KKT conditions

Since we have shown that the modified standard optimization formulation in (4) is convex, its KKT conditions are both necessary and sufficient optimality conditions. To derive the KKT conditions, the Lagrangian of (4) takes the following form by introducing a Lagrange multiplier ϕ corresponding to the volume constraint:

$$\mathcal{L}(\boldsymbol{x}, \phi) = J(\boldsymbol{x}) + \phi \left(\sum_{i=1}^{n} x^{(i)} L^{(i)} - V_{\max} \right). \tag{13}$$

[4]Both Odgen-based and bilinear materials with the condition $\mathrm{d}\sigma(\lambda)/\mathrm{d}\lambda \geq 0$ have convex specific strain energy – see Section 3.1 for constraints on the model parameters.

[5]Notice that the theoretical unbounded solution is represented by a numerical solution displaying infeasible displacements (i.e., relatively large values).

[6]The given random vector $\boldsymbol{x}_r = [7.78, 7.23, 0.76, 4.30, 0.38, 9.25, 3.80, 5.05, 6.94, 3.99, 6.77, 5.24, 7.74, 3.41, 6.10, 9.73, 5.44, 6.33, 2.32, 5.19]^T$. In the full-order model, the filtered vector $\boldsymbol{x}_{rf} = [7.78, 7.23, 0, 4.30, 0, 9.25, 0, 5.05, 6.94, 3.99, 6.77, 5.24, 7.74, 0, 6.10, 9.73, 5.44, 6.33, 0, 5.19]^T$. In the reduced-order model, the filtered vector $\boldsymbol{x}_{rf} = [7.78, 7.23, 4.30, 9.25, 5.05, 6.94, 3.99, 6.77, 5.24, 7.74, 6.10, 9.73, 5.44, 6.33, 5.19]^T$. For related content, see Section 4 (and Fig. 6).

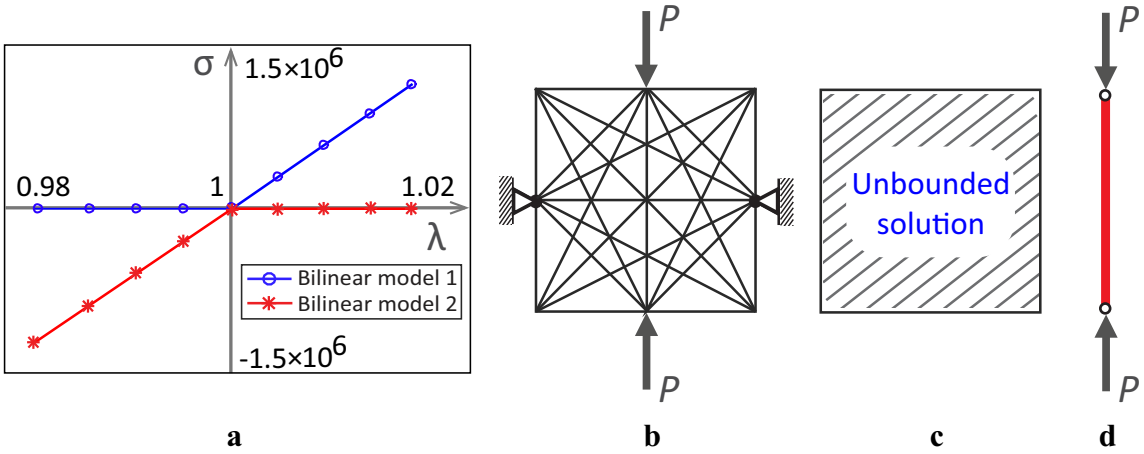

Fig. 4 Topology optimization: unbounded versus bounded solutions. **a** Bilinear material models; **b** initial ground structure and boundary conditions; **c** the tension-dominated "bilinear model 1" leads to an unbounded solution because the structural model cannot carry the loads (the equilibrium condition is not satisfied, i.e., $\boldsymbol{T}(\boldsymbol{x}, \boldsymbol{u}(\boldsymbol{x})) \neq \boldsymbol{F}$) with this material model; **d** the compression-dominated "bilinear model 2" leads to a bounded solution and self-equilibrated structure

If we denote $\boldsymbol{x}^*$ as the optimal solution of design variables, and ϕ^* as the optimal solution for the Lagrange multiplier, we have (Christensen and Klarbring 2009),

$$\frac{\partial \mathcal{L}}{\partial x^{(i)}}\left(\boldsymbol{x}^*, \phi^*\right) \leq 0, \quad \text{if} \quad x^{(i)^*} = x_{\max}^{(i)}, \tag{14}$$

$$\frac{\partial \mathcal{L}}{\partial x^{(i)}}\left(\boldsymbol{x}^*, \phi^*\right) = 0, \quad \text{if} \quad 0 < x^{(i)^*} < x_{\max}^{(i)}, \tag{15}$$

$$\frac{\partial \mathcal{L}}{\partial x^{(i)}}\left(\boldsymbol{x}^*, \phi^*\right) \geq 0, \quad \text{if} \quad x^{(i)^*} = 0, \tag{16}$$

where the derivative of the Lagrangian is given by

$$\frac{\partial \mathcal{L}}{\partial x^{(i)}}(\boldsymbol{x}, \phi) = -\sum_{j=1}^{m} w_j L^{(i)} \Psi^{(i)}\left(\boldsymbol{u}_j(\boldsymbol{x})\right) + \phi L^{(i)}. \tag{17}$$

Combining (17) with (14)–(16), we obtain the KKT conditions for the optimal solution $(\boldsymbol{x}^*, \phi^*)$ of the optimization formulation in (4):

$$\sum_{j=1}^{m} w_j \Psi^{(i)}\left(\boldsymbol{u}_j(\boldsymbol{x}^*)\right) \geq \phi^*, \quad \text{if} \quad x^{(i)^*} = x_{\max}^{(i)}, \tag{18}$$

$$\sum_{j=1}^{m} w_j \Psi^{(i)}\left(\boldsymbol{u}_j(\boldsymbol{x}^*)\right) = \phi^*, \quad \text{if} \quad 0 < x^{(i)^*} < x_{\max}^{(i)}, \tag{19}$$

$$\sum_{j=1}^{m} w_j \Psi^{(i)}\left(\boldsymbol{u}_j(\boldsymbol{x}^*)\right) \leq \phi^*, \quad \text{if} \quad x^{(i)^*} = 0. \tag{20}$$

From (19), we observe that for those members whose optimal design variables fall between the upper and lower bounds (with inactive area constraints), the weighted sums of the corresponding specific strain energy over m load cases in the optimal topology are identical, which equal to ϕ^*. Moreover, we note that under the single load case, i.e., $m = 1$, (19) implies that the specific strain energy for all the members with inactive area constraints in the optimal topology is identical (Khot and Kamat 1985; Ramos Jr and Paulino 2015), which corresponds to the full stress design in the linear case (Christensen and Klarbring 2009).

3 Truss model with material nonlinearity

We present the theory in which the structural analysis part of the paper is based upon. This includes the kinematics, hyperelastic constitutive models, the potential energy, the linearization of the nonlinear equations, the Tikhonov regularization, and the line search. In fact, the use of line search to solve topology optimization problems governed by nonlinear state equations is an important aspect of this work.

3.1 Kinematics and constitutive models

To construct the kinematics and constitutive models, we assume small deformation kinematics and nonlinear constitutive relationships. For a given truss element, its linearized stretch λ is computed as (Bonet and Wood 2008)

$$\lambda = 1 + \frac{\boldsymbol{N}^{\mathrm{T}}\left(\boldsymbol{u}_q - \boldsymbol{u}_p\right)}{L}, \tag{21}$$

where $\boldsymbol{u}_p$ and $\boldsymbol{u}_q$ are the nodal displacement vectors of nodes p and q of the truss element, $\boldsymbol{N}$ is the member's unit directional vector, and L is the length of the element. To account for the nonlinear constitutive relation, we use the energy density function based on Ogden (1984), which provides flexibility to specify the material behavior and thus has the capability to reproduce a variety

of hyperelastic models. For the hyperelastic Ogden material, the strain energy per unit of the undeformed volume is given as

$$\Psi_{OG}\left(\lambda_1,\lambda_2,\lambda_3\right)=\sum_{j=1}^{M}\frac{\gamma_j}{\beta_j}\left(\lambda_1^{\beta_j}+\lambda_2^{\beta_j}+\lambda_3^{\beta_j}-3\right), \quad (22)$$

where $\lambda_i,\ i=1,2,3$, denote the principal stretches in three directions, and M, γ_j, and β_j are material parameters (constants). We assume that the axial stretch of the truss member is the principal stretch λ_1, namely, $\lambda_1=\lambda$, and the stretches in the other two directions are taken to be $\lambda_2=\lambda_3=1$, such that (22) becomes

$$\hat{\Psi}_{OG}\left(\lambda\right)=\sum_{j=1}^{M}\frac{\gamma_j}{\beta_j}\left(\lambda^{\beta_j}-1\right). \quad (23)$$

Accordingly, the principal (Cauchy) stress for the Ogden-based model is obtained as

$$\sigma_{OG,1}=\frac{\partial\Psi_{OG}}{\partial\lambda_1}\ \text{ and }\ \sigma_{OG,2}=\sigma_{OG,3}=0. \quad (24)$$

Throughout this work, the energy density function is used with $M=2$; thus, we obtain

$$\sigma_{OG}\left(\lambda\right)=\frac{\mathrm{d}\hat{\Psi}_{OG}}{\mathrm{d}\lambda}\left(\lambda\right)=\gamma_1\left(\lambda^{\beta_1-1}-\lambda^{\beta_2-1}\right), \quad (25)$$

with $\gamma_2=-\gamma_1$. By taking the derivative of the stress, the tangent modulus is obtained as follows:

$$E_T\left(\lambda\right)=\frac{\mathrm{d}\sigma_{OG}}{\mathrm{d}\lambda}\left(\lambda\right)=\gamma_1\left[\left(\beta_1-1\right)\lambda^{\beta_1-2}-\left(\beta_2-1\right)\lambda^{\beta_2-2}\right]. \quad (26)$$

Notice that, at undeformed state, the tangent modulus reduces to the Young's modulus in linear elasticity, namely,

$$E_T\left(1\right)=\gamma_1\left(\beta_1-\beta_2\right)=E_0=\Lambda+2\mu, \quad (27)$$

where Λ and μ are the usual Lamé constants.

In terms of the convexity of this Ogden-based material model, if the parameters satisfy the following conditions: $\beta_1\geq 1$, $\beta_2\leq 1$, $\beta_1\neq\beta_2$, and $\gamma_1>0$, which results in $E_T>0$ ($\mathrm{d}\sigma_{OG}\left(\lambda\right)/\mathrm{d}\lambda>0$), then the material model is convex, i.e., $\hat{\Psi}_{OG}\left(\lambda\right)$ is convex for $\lambda>0$. The material parameters $(\beta_1,\beta_2,\gamma_1)$ are solved using (27) and the relation

$$\frac{\sigma_t}{\sigma_c}=\frac{\overline{\sigma}_t}{\overline{\sigma}_c}, \quad (28)$$

where

$$\overline{\sigma}_t=\frac{\sigma_t}{\gamma_1^0}=\left(\lambda_t^{\beta_1-1}-\lambda_t^{\beta_2-1}\right)\ \text{ and }\ \overline{\sigma}_c=\frac{\sigma_c}{\gamma_1^0}=\left(\lambda_c^{\beta_1-1}-\lambda_c^{\beta_2-1}\right). \quad (29)$$

Note that σ_t, σ_c, E_0, λ_t, λ_c and γ_1^0 are specified by the user. Therefore, the stress-stretch relationship of the Ogden model is obtained as,

$$\sigma_{OG}\left(\lambda\right)=\frac{E_0}{\beta_1-\beta_2}\left(\lambda^{\beta_1-1}-\lambda^{\beta_2-1}\right). \quad (30)$$

By varying the set of parameters (β_1,β_2), this Ogden-based model generates a variety of material behavior, as shown in Fig. 5a.

In this work, we also adopt a bilinear material to account for constitutive relationships. The bilinear constitutive model has a kink at the origin (see Fig. 5b). To treat this class of nonsmooth problems, we refer the reader to Klarbring and Rönnqvist (1995). Within the same context of the Ogden-based model, the energy density function can be written as,

$$\Psi_{Bi}\left(\lambda\right)=\begin{cases}\frac{1}{2}E_t\left(\lambda-1\right)^2, & \text{if } \lambda>1,\\ \frac{1}{2}E_c\left(\lambda-1\right)^2, & \text{otherwise,}\end{cases} \quad (31)$$

where E_t and E_c are the Young's moduli for tension and compression, respectively. Accordingly, the Cauchy stress for the bilinear material is then obtained as,

$$\sigma_{Bi}\left(\lambda\right)=\begin{cases}E_t\left(\lambda-1\right), & \text{if } \lambda>1,\\ E_c\left(\lambda-1\right), & \text{otherwise.}\end{cases} \quad (32)$$

Note that this bilinear material model is always convex as $\mathrm{d}\sigma_{\mathrm{Bi}}\left(\lambda\right)/\mathrm{d}\lambda\geq 0$. The term $\mathrm{d}\sigma_{\mathrm{Bi}}\left(\lambda\right)/\mathrm{d}\lambda$ may become zero, which occurs, for example, when the material that is unable to carry compression (e.g., cables, $E_c=0$), that is $\mathrm{d}\sigma_{\mathrm{Bi}}\left(\lambda\right)/\mathrm{d}\lambda=0$ in the compression range.

3.2 Potential energy

A brief derivation of the equilibrium equations is given here for the sake of completeness–details of the derivation were reviewed in Ramos Jr and Paulino (2015). By definition, the standard total potential energy of the structure is $\Pi\left(\boldsymbol{u}\right)=U\left(\boldsymbol{u}\right)+\Omega\left(\boldsymbol{u}\right)$. The equilibrium of the structure is enforced by requiring Π to be stationary; that is,

$$\boldsymbol{R}\left(\boldsymbol{u}\right)=\frac{\partial U}{\partial\boldsymbol{u}}+\frac{\partial\Omega}{\partial\boldsymbol{u}}=\boldsymbol{T}\left(\boldsymbol{u}\right)-\boldsymbol{F}=0, \quad (33)$$

where $\boldsymbol{T}\left(\boldsymbol{u}\right)$ is the internal force vector in terms of the state variable $\boldsymbol{u}$, and $\boldsymbol{F}$ is the external force vector. The internal force vector $\boldsymbol{T}\left(\boldsymbol{u}\right)$ is given as,

$$\boldsymbol{T}\left(\boldsymbol{u}\right)=\sum_{i=1}^{n}x^{(i)}L^{(i)}\frac{\partial\Psi^{(i)}}{\partial\boldsymbol{u}}. \quad (34)$$

In the above relation, $\partial\Psi^{(i)}/\partial\boldsymbol{u}$ is obtained as

$$\frac{\partial\Psi^{(i)}}{\partial\boldsymbol{u}}=\frac{\mathrm{d}\Psi^{(i)}}{\mathrm{d}\lambda^{(i)}}\frac{\partial\lambda^{(i)}}{\partial\boldsymbol{u}}. \quad (35)$$

Using (21), we obtain

$$\frac{\partial\lambda^{(i)}}{\partial\boldsymbol{u}}=\frac{1}{L^{(i)}}\begin{Bmatrix}\vdots\\ -\boldsymbol{N}^{(i)}\\ \vdots\\ \boldsymbol{N}^{(i)}\\ \vdots\end{Bmatrix}=\frac{1}{L^{(i)}}\boldsymbol{B}^{(i)},\ \text{ where }\boldsymbol{B}^{(i)}=\begin{Bmatrix}\vdots\\ -\boldsymbol{N}^{(i)}\\ \vdots\\ \boldsymbol{N}^{(i)}\\ \vdots\end{Bmatrix}. \quad (36)$$

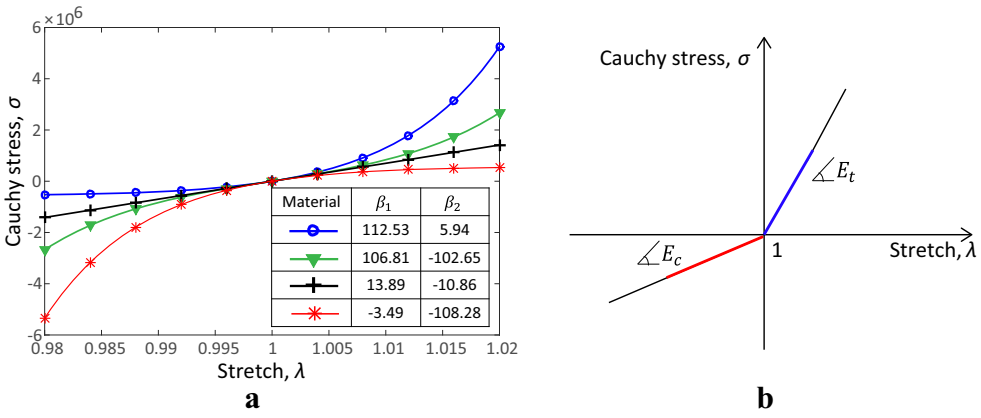

Fig. 5 Material models: **a** Hyperelastic Ogden-based models with different parameters (β_1, β_2); **b** bilinear material model with elastic behavior (different Young's moduli for tension and for compression)

Therefore, the local internal force vector is obtained by substituting (35) and (36) into (34), which gives

$$\boldsymbol{T}(\boldsymbol{u}) = \sum_{i=1}^{n} x^{(i)} \sigma^{(i)} \boldsymbol{B}^{(i)}. \tag{37}$$

3.3 Linearization of the nonlinear algebraic equations (Newton-Raphson method)

In solving the nonlinear system of equations, the residual force $\boldsymbol{R}(\boldsymbol{u})$ of (33) can be linearized and rewritten for iteration k as follows:

$$\boldsymbol{R}\left(\boldsymbol{u}^{k+1}\right) = \boldsymbol{R}\left(\boldsymbol{u}^{k}\right) + \boldsymbol{K}_t\left(\boldsymbol{u}^{k}\right)\Delta\boldsymbol{u}^{k}, \tag{38}$$

where $\boldsymbol{K}_t$ is the global tangent stiffness matrix,

$$\boldsymbol{K}_t\left(\boldsymbol{u}^{k}\right) = \frac{\partial \boldsymbol{R}}{\partial \boldsymbol{u}}\left(\boldsymbol{u}^{k}\right) = \frac{\partial \boldsymbol{T}}{\partial \boldsymbol{u}}\left(\boldsymbol{u}^{k}\right). \tag{39}$$

The nonlinear structural problem is solved using the Newton-Raphson method (Wriggers 2008) :

$$\boldsymbol{R}\left(\boldsymbol{u}^{k+1}\right) = \boldsymbol{R}\left(\boldsymbol{u}^{k}\right) + \boldsymbol{K}_t\left(\boldsymbol{u}^{k}\right)\Delta\boldsymbol{u}^{k} = 0, \tag{40}$$

therefore,

$$\boldsymbol{K}_t\left(\boldsymbol{u}^{k}\right)\Delta\boldsymbol{u}^{k} = -\boldsymbol{R}\left(\boldsymbol{u}^{k}\right) = \boldsymbol{F} - \boldsymbol{T}\left(\boldsymbol{u}^{k}\right), \tag{41}$$

and

$$\boldsymbol{u}^{k+1} = \boldsymbol{u}^{k} + \Delta\boldsymbol{u}^{k}, \tag{42}$$

where $\boldsymbol{K}_t = \sum_{i=1}^{n} \boldsymbol{K}_t^{(i)}$, and $\boldsymbol{K}_t^{(i)}$ is the element tangent stiffness matrix in global coordinates. For a given truss element i with nodes p and q, the associated internal force vector $\boldsymbol{t}^{(i)}$ and local tangent stiffness matrix $\boldsymbol{k}_t^{(i)}$ are expressed as follows:

$$\boldsymbol{t}^{(i)}\left(\boldsymbol{u}^{(i)}\right) = x^{(i)}\sigma^{(i)}\left(\boldsymbol{u}^{(i)}\right)\begin{Bmatrix} -\boldsymbol{N}^{(i)} \\ \boldsymbol{N}^{(i)} \end{Bmatrix}, \tag{43}$$

and

$$\boldsymbol{k}_t^{(i)} = \frac{\partial \boldsymbol{t}^{(i)}}{\partial \boldsymbol{u}^{(i)}} = \begin{bmatrix} \boldsymbol{k}_{pp} & \boldsymbol{k}_{pq} \\ \boldsymbol{k}_{qp} & \boldsymbol{k}_{qq} \end{bmatrix}, \tag{44}$$

where

$$\boldsymbol{k}_{pp} = \boldsymbol{k}_{qq} = -\boldsymbol{k}_{pg} = -\boldsymbol{k}_{qp} = \frac{x^{(i)}}{L^{(i)}}\frac{\mathrm{d}\sigma^{(i)}}{\mathrm{d}\lambda^{(i)}}\boldsymbol{N}^{(i)}\left(\boldsymbol{N}^{(i)}\right)^{\mathrm{T}}. \tag{45}$$

3.4 Solving the state equations: Tikhonov regularization

To prevent the possibility of a singular tangent stiffness matrix from forming in the Newton-Raphson method of the structural nonlinear equations in the proposed scheme, we introduce a regularization term (Tikhonov and Arsenin 1977; Felippa n.d; Ramos Jr and Paulino 2016; Talischi and Paulino 2013). The total potential energy accounting for the Tikhonov regularization term is written as

$$\Pi^{\eta}(\boldsymbol{u}) = U(\boldsymbol{u}) + \Omega(\boldsymbol{u}) + \frac{\eta}{2}\boldsymbol{u}^{\mathrm{T}}\boldsymbol{u}, \tag{46}$$

where η is a positive Tikhonov regularization parameter. By taking the derivative of the above equation,

$$\boldsymbol{R}^{\eta}(\boldsymbol{u}) = \frac{\partial \Pi^{\eta}}{\partial \boldsymbol{u}} = \frac{\partial U}{\partial \boldsymbol{u}} + \frac{\partial \Omega}{\partial \boldsymbol{u}} + \eta\boldsymbol{u} = \boldsymbol{T}(\boldsymbol{u}) - \boldsymbol{F} + \eta\boldsymbol{u} = 0. \tag{47}$$

In the Newton-Raphson method, the residual force $\boldsymbol{R}^{\eta}(\boldsymbol{u})$ of (47) can be rewritten for the iteration $k+1$ as follows:

$$\boldsymbol{R}^{\eta}\left(\boldsymbol{u}^{k+1}\right) = \boldsymbol{R}^{\eta}\left(\boldsymbol{u}^{k} + \Delta\boldsymbol{u}^{k}\right) = \boldsymbol{R}^{\eta}\left(\boldsymbol{u}^{k}\right) + \frac{\partial \boldsymbol{R}^{\eta}\left(\boldsymbol{u}^{k}\right)}{\partial \boldsymbol{u}^{k}}\Delta\boldsymbol{u}^{k}, \tag{48}$$

where

$$\frac{\partial \boldsymbol{R}^{\eta}\left(\boldsymbol{u}^{k}\right)}{\partial \boldsymbol{u}^{k}} = \boldsymbol{K}_t\left(\boldsymbol{u}^{k}\right) + \eta\boldsymbol{I}. \tag{49}$$

Hence, the linearized equilibrium equation of the nonlinear system becomes

$$\left[\boldsymbol{K}_t\left(\boldsymbol{u}^{k}\right) + \eta\boldsymbol{I}\right]\Delta\boldsymbol{u}^{k} = \boldsymbol{F} - \boldsymbol{T}\left(\boldsymbol{u}^{k}\right) - \eta\boldsymbol{u}^{k}. \tag{50}$$

In above equations, the term $\eta \boldsymbol{I}$ is the regularization term for the tangent stiffness matrix. We select the value of η as

$$\eta = \frac{\eta_0}{N} \mathrm{tr}\left(\boldsymbol{K}_{t,\mathrm{Top}}\right), \tag{51}$$

where typically $\eta_0 = 10^{-8}$, and $\boldsymbol{K}_{t,\mathrm{Top}}$ is the stiffness matrix of the filtered structure that will be discussed in the subsequent section. Note that the term $\eta \boldsymbol{u}^k$ on the right-hand side of (50) can be neglected since η has relatively small value and we seek to satisfy equilibrium condition, $\boldsymbol{T}\left(\boldsymbol{u}^k\right) = \boldsymbol{F}$.

3.5 Inexact line search

In an effort to improve the convergence of the first several iterations of the nonlinear FEM (the structural configuration tends to be more flexible than the solution being sought), we adopt an inexact (Armijo-type) line search strategy (Armijo 1966; Bertsekas 1999; Ascher and Greif 2011) within the Newton-Raphson procedure, which modifies (42) to

$$\boldsymbol{u}^{k+1} = \boldsymbol{u}^k + \xi^k \Delta \boldsymbol{u}^k. \tag{52}$$

A scalar step length ξ^k is calculated in each iteration, which guarantees a decrease in the potential energy, $\Pi\left(\boldsymbol{u}^{k+1}\right)$. The rationale is to search along $\boldsymbol{u}^k + \xi \Delta \boldsymbol{u}^k$ to find $\xi = \xi^k$ such that

$$\Pi\left(\boldsymbol{u}^{k+1}\right) = \Pi\left(\boldsymbol{u}^k + \xi^k \Delta \boldsymbol{u}^k\right) \leq \Pi\left(\boldsymbol{u}^k\right) + \tau \xi^k \nabla \Pi\left(\boldsymbol{u}^k\right)^{\mathrm{T}} \Delta \boldsymbol{u}^k, \tag{53}$$

where τ is the guard constant, e.g., $\tau = 10^{-4}$. Note that $\nabla \Pi\left(\boldsymbol{u}^k\right) = \boldsymbol{R}\left(\boldsymbol{u}^k\right)$. If the current step length $\bar{\xi}^k$ is unsatisfactory, the following procedure is used to decrease the step length. We first calculate a quadratic polynomial and minimize the interpolant based on (53), obtaining a scale κ of the step length for the next potential step length:

$$\kappa = -\frac{\bar{\xi}^k \nabla \Pi\left(\boldsymbol{u}^k\right)^{\mathrm{T}} \Delta \boldsymbol{u}^k}{2\left(\Pi\left(\boldsymbol{u}^k + \bar{\xi}^k \Delta \boldsymbol{u}^k\right) - \Pi\left(\boldsymbol{u}^k\right) - \bar{\xi}^k \nabla \Pi\left(\boldsymbol{u}^k\right)^{\mathrm{T}} \Delta \boldsymbol{u}^k\right)}, \tag{54}$$

and updating ξ^k as $\xi^k = \kappa \bar{\xi}^k$. If a relatively small scalar value, e.g., $\kappa < 0.1$, is obtained, we simply use $\kappa = 0.5$. Under the assumptions in Section 2.1, the Newton-Raphson method with this line search method ensures the convergence to a displacement field that is a stationary point (Bertsekas 1999) in the potential energy. Furthermore, if the potential energy is strictly convex with respect to $\boldsymbol{u}$, which is the case in our paper with the Tikhonov regularization, then the stationary point ($\boldsymbol{u}$) is the unique global minimum.

4 Reduced-order model

This section introduces the fully reduced-order model (ROM) in nonlinear topology optimization with GSM using the discrete filter. The ROM is applied to both the nonlinear structural system analysis (the state problem) and the optimization analysis.

4.1 Reduced-order model in nonlinear structural system analysis

Utilizing the reduced-order model, after each filtering process, we form a reduced-sized structure and a new set of degrees of freedom (DOFs). The subscript (Top) represents the new set of variables associated with the filtered structure. Solving the nonlinear structural problem requires filtering out the topology from the ground structure based on the following mapping of variables:

$$\boldsymbol{u} = \boldsymbol{Q}\boldsymbol{u}_{\mathrm{Top}}, \tag{55}$$

where the matrix $\boldsymbol{Q}$ maps the DOFs between the ground structure and the actual topology after applying the filter. This matrix is defined based on the nodes connected with those elements with finite cross-sectional area value (larger than zero) and the associated new set of DOFs. Based on this mapping, we establish the associated structural problem as follows (Ramos Jr and Paulino 2016):

$$\boldsymbol{T}_{\mathrm{Top}}\left(\boldsymbol{u}_{\mathrm{Top}}\right) = \boldsymbol{F}_{\mathrm{Top}}, \tag{56}$$

$$\left(\boldsymbol{K}_{t,\mathrm{Top}} + \eta \mathbf{I}\right) \Delta \boldsymbol{u}^k_{\mathrm{Top}} = \boldsymbol{F}_{\mathrm{Top}} - \boldsymbol{T}^k_{\mathrm{Top}} = \boldsymbol{R}^k_{\mathrm{Top}}, \tag{57}$$

and

$$\boldsymbol{u}^{k+1}_{\mathrm{Top}} = \boldsymbol{u}^k_{\mathrm{Top}} + \Delta \boldsymbol{u}^k_{\mathrm{Top}}, \tag{58}$$

where $\boldsymbol{K}_{t,\mathrm{Top}}$, $\boldsymbol{F}_{\mathrm{Top}}$, and $\boldsymbol{T}^k_{\mathrm{Top}}$ are the tangent stiffness, the external and internal load vectors, respectively, associated with the actual topology, defined by

$$\boldsymbol{K}_{t,\mathrm{Top}} = \boldsymbol{Q}^{\mathrm{T}} \boldsymbol{K}_t \boldsymbol{Q}, \quad \boldsymbol{F}_{\mathrm{Top}} = \boldsymbol{Q}^{\mathrm{T}} \boldsymbol{F}, \quad \text{and} \quad \boldsymbol{T}^k_{\mathrm{Top}} = \boldsymbol{Q}^{\mathrm{T}} \boldsymbol{T}^k. \tag{59}$$

For simplicity, we use notations $\boldsymbol{T}^k$, $\boldsymbol{T}^k_{\mathrm{Top}}$, and $\boldsymbol{R}^k_{\mathrm{Top}}$ to denote $\boldsymbol{T}\left(\boldsymbol{u}^k\right)$, $\boldsymbol{T}_{\mathrm{Top}}\left(\boldsymbol{u}^k_{\mathrm{Top}}\right)$, and $\boldsymbol{R}_{\mathrm{Top}}\left(\boldsymbol{u}^k_{\mathrm{Top}}\right)$. A mapping example for the ROM in the nonlinear structural system analysis is presented in Appendix B. The tangent stiffness matrix from the formulation in (7) can be singular when truss members are removed. Therefore, we minimize the potential energy with the Tikhonov regularization. After solving for $\boldsymbol{u}_{\mathrm{Top}}$, we use this displacement field to calculate the sensitivity of the filtered structure. Thus, for the proposed filtering scheme, during and after the optimization process we check the global equilibrium residual by

$$||\boldsymbol{R}^k_{\mathrm{Top}}|| \leq \rho ||\boldsymbol{F}_{\mathrm{Top}}||, \tag{60}$$

where ρ represents the tolerance. We choose the value of ρ as 10^{-4} throughout this paper. For the standard GSM, we check the global equilibrium residual on the structure after applying the final cut-off, i.e. a posteriori. For the linear cases with the filter that are used in the examples, we check the global equilibrium residual using

$$||\boldsymbol{K}_{\text{Top}}\boldsymbol{u}_{\text{Top}} - \boldsymbol{F}_{\text{Top}}|| \leq \rho||\boldsymbol{F}_{\text{Top}}||. \tag{61}$$

We remove information about the deleted members, including the areas, stiffness matrix, from the problem. We do not simply set areas of the removed members to zero or store nodes, but instead, remove the information from the entire problem, as shown in Fig. 6. This reduced number of truss members significantly influences the size of the global stiffness matrix. Typically, the formation and inversion of the stiffness matrix is one of the most time-consuming parts of nonlinear FEM. To quantify the influence of using the ROM, we conduct studies in Sections 5.1 and 5.3. As we will see, the size of the problem significantly decreases as the iteration proceeds.

The application of the filtering scheme with the ROM in truss optimization that accounts for material nonlinearity has the advantage of solving structural problems in the filtered topology. As a result of the smaller sizes of the tangent stiffness matrices, the use of the ROM incorporated into the proposed scheme significantly improves the performance of the computations in the iterative Newton-Raphson algorithm.

4.2 Reduced-order model in optimization analysis

To reduce the order of information needed in the sensitivity analysis and update scheme to achieve fully reduced-order in the entire optimization process, we further use the reduced-order model in the optimization analysis, because we assume that the null area members do not return to the topology. This situation is automatically considered by the construction of the optimality criteria (OC) (Groenwold and Etman 2008), which is the update scheme that we choose. The size of the information input for the update (i.e., vectors of sensitivity and design variables) is the same as that used for solving the nonlinear structural system. Note that the proposed scheme uses reduced-order information in sensitivity and design variable vectors with the removal of information associated with null-area members; this excludes the sensitivity information of members with zero areas but non-zero nodal displacement (because according to (9), the sensitivities of those null-area members are not zero). As a result, regardless of which update scheme is adopted (the optimality criteria or the method of moving asymptotes (MMA) by Svanberg 1987), the removed members will not return to the topology once they have been removed. Therefore, although the OC by its construction does not allow the return of the members, it is sufficient for the reduced-order model and is adopted in this paper.

However, we note that the return of the bars may be helpful when a large filter value is used. Application of a large filter may lead to the removal of many bars, and thus the resulting structure may not be in equilibrium, or the objective may increase dramatically (large displacement). For instance, if some structurally important members are removed, large displacements may occur. In such cases, the excluded sensitivity information is potentially useful for accomplishing the optimization and maintaining equilibrium, in which case the MMA could be used, which enables the return of the bars.

5 Numerical examples

This section illustrates the proposed formulation using four representative examples. The first example verifies the methodology in two dimensions; the second example demonstrates how altering the material constitutive relation changes the final topology. Then we compare the optimized structures from the proposed scheme under single and multiple load cases with those from the linear plastic formulation under single load case. The last two examples, which are in three dimensions, establish the capability of the proposed method, including a practical structural design with various materials. All of the examples, except Example 2, use hyperelastic Ogden-based materials under small displacements. Example 2 uses bilinear material models. The examples are illustrated by Table 1.

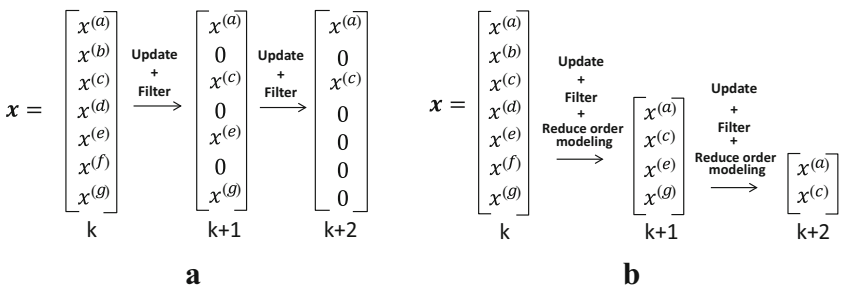

Fig. 6 Evolution of the design variables during the optimization process: **a** full-order model; **b** reduced-order model

Table 1 Numerical examples

Example	Dimension	Description	Feature
1	2D	Central load in a simply supported square domain	Verification
2	2D	Long-span bridge design using bilinear materials	Comparison of elastic and plastic formulations of the ground structure
3	3D	Central load on the top surface of a laterally constrained parallelepiped	Influence of load level in the nonlinear response
4	3D	Arch bridge	Potentially translational design: from academia to structural engineering practice

For all of the examples, we generate the initial ground structure and remove overlapped bars (Bensøe and Sigmund 2003). For the generation of three-dimensional (3D) initial ground structures and the plotting of the 3D final structures, we employ the software GRAND3 and the collision zone technique by Zegard and Paulino (2014) and Zegard and Paulino (2015b). The CPU run-time in this paper reflects the time spent on the optimization process, not including the time spent on problem formulation. Both the standard GSM in (3) with a final cut-off and the proposed filter formulation in (7) may lead to structures with aligned nodes, i.e., hinges connecting two collinear members that cause mechanism. In this work, for the standard formulation after the final cut-off, we remove aligned nodes (and floating members) by replacing two collinear members with one long member that takes the larger area from the two, and the resulting objective value decreases. For the proposed filter, we remove aligned nodes by replacing the two collinear members with one long member that takes the same area, and the resulting objective value stays unchanged. All the data presented in this paper are obtained after removing aligned nodes. For both methods, we check the final topologies to ensure that they are at equilibrium. However, we do not verify the instability of the members because the issue of stability is beyond the scope of this work. All examples have the initial tangent modulus, $E_0 = 7 \times 10^7 (= E_t$ for Example 2); the stopping criteria: $\text{tol}_{\text{opt}} = 10^{-9}$; move value: $10^4 x^0$, where x^0 is the initial guess of the design variables. For the standard GSM, we apply a cut-off value that defines the final structure at the end of the optimization process; the cut-off value for Examples 1 and 3 is 10^{-2} for the cases that use the standard GSM. For the cases with the proposed filtering scheme, we use a relatively small filter, $\alpha_f = 10^{-4}$, in all the examples during the optimization process, and the filter operation is performed at every optimization step, i.e., $N_f = 1$. The lower and upper bounds for the standard GSM are defined by $x_{\min} = 10^{-2} x^0$ and $x_{\max} = 10^4 x^0$, respectively. For the proposed filter algorithm, $x_{\min} = 0$ and $x_{\max} = 10^4 x^0$ (unbounded in practical terms).

5.1 Example 1: Central load in a simply supported square domain

The purpose of Example 1 is to verify the present methodology with the results obtained from standard GSM using two hyperelastic Ogden-based material models without the filtering scheme (Ramos Jr and Paulino 2015). We also study the influence of material models on the resulting structural topology by comparing the two Ogden-based models with a linear model. The geometry, load, and support conditions

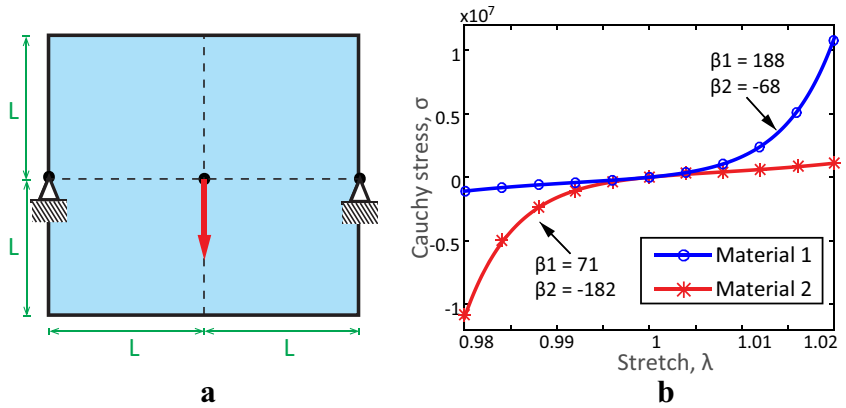

Fig. 7 Example 1 with a full-level ground structure (12 × 12 grid) and 6,920 non-overlapped bars: **a** Geometry ($L = 6m$), load ($P = 100kN$) and support conditions; **b** Ogden-based material models. Material 1 is tension dominated, while Material 2 is compression dominated (online version in color)

(two fixed supports) are shown in Fig. 7a. The initial ground structure contains 6,920 non-overlapped members and 169 nodes using full-level generation. We use two Ogden-based material models, illustrated in Fig. 7b. The figure shows that the tension of Material 1 ($\beta_1 = 188, \beta_2 = -68$) is stronger than its compression, and the compression of Material 2 ($\beta_1 = 71, \beta_2 = -182$) is stronger than its tension. We use a small filter $\alpha_f = 10^{-4}$ throughout the optimization process.

The filtering scheme yields topologies almost identical to those obtained using the standard GSM with a final cut-off for both linear and nonlinear materials, as shown in Fig. 8, and in the paper by Ramos Jr and Paulino (2015). This comparison verifies the proposed filtering scheme. The choice of material models significantly influences the final topology. Note that each material model results in a unique topology, and each differs from the linear case. If a material used in practical design exhibits nonlinear behavior, an analysis based on a linear material may be misleading. Various topologies resulting from the use of several materials show the importance of accounting for material nonlinearity. In addition, since single load case is used here, we observe that in every model considering

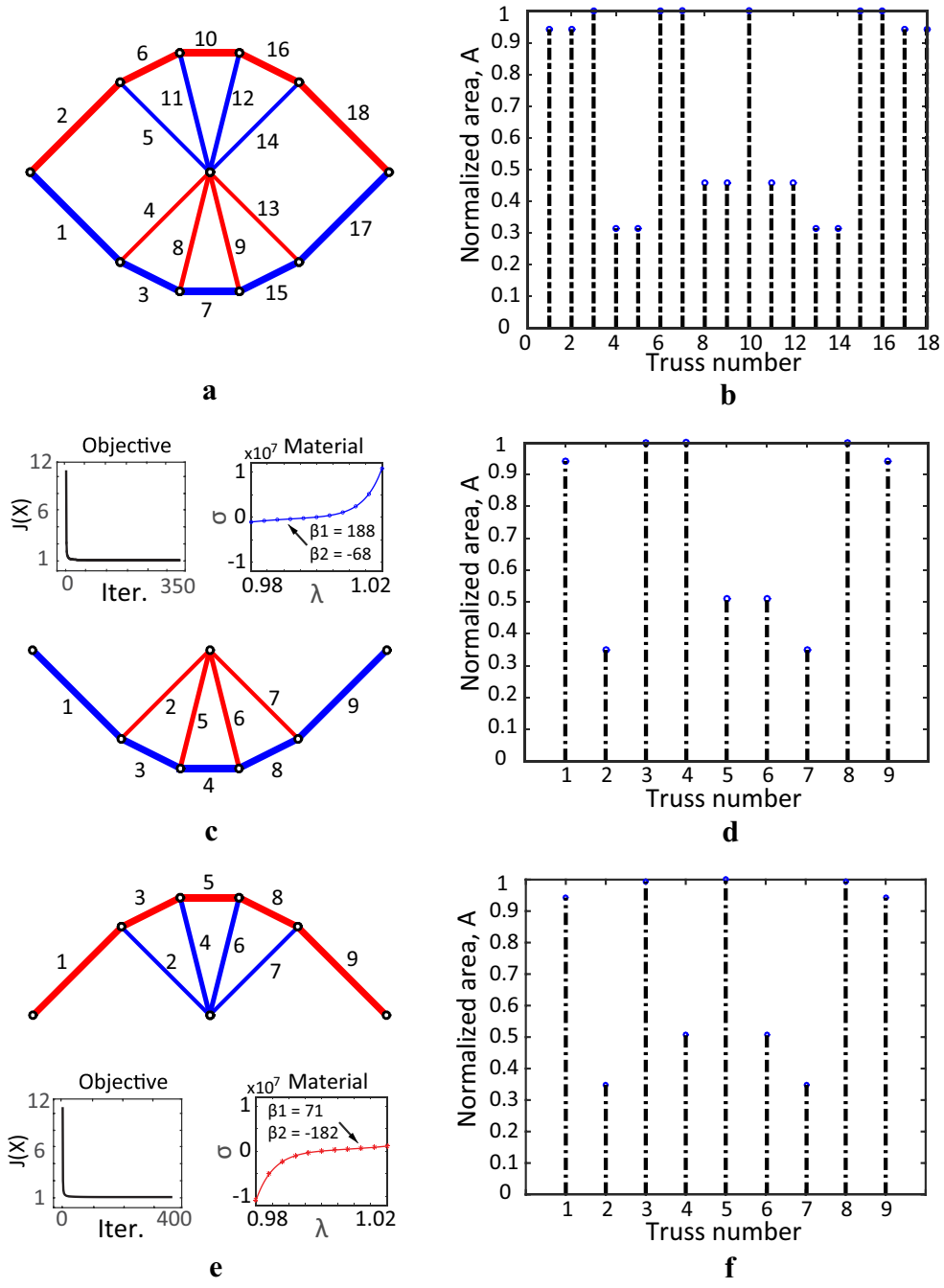

Fig. 8 Results of the optimization for Example 1: **a** Final topology of the linear model; **b** corresponding final normalized cross-sectional areas for the truss members of the linear model; **c** final topology and convergence plot for Ogden-based "Material 1" (tension-dominated); **d** corresponding final normalized cross-sectional areas for truss members of Ogden-based "Material 1"; **e** final topology and convergence plot for Ogden-based "Material 2" (compression-dominated); **f** corresponding final normalized cross-sectional areas for truss members of Ogden-based "Material 2". The *blue bars* are in tension and the *red bars* are under compression (online version in color)

Table 2 Numerical information for Example 1 (Fig. 7)

Model	$J(\boldsymbol{x}^*)$ $(\text{kN}\cdot m)$	$\Psi(\boldsymbol{u}(\boldsymbol{x}^*))$ (kN/m^2)	Max$\lvert\boldsymbol{u}\rvert$ (cm)	Max λ	Min λ	# Opt. Steps	CPU (sec)	α_f	α_{Top}	Equilibrium Residual
Linear (Filter)	1.096	68.48	2.19	1.0014	0.9986	465	20	10^{-4}	0.3143	1.00×10^{-13}
Mat.1 (Filter)	1.073	65.62	2.12	1.0013	0.9986	353	24	10^{-4}	0.3494	1.10×10^{-13}
Mat.2 (Filter)	1.073	65.67	2.12	1.0014	0.9987	355	24	10^{-4}	0.3485	1.83×10^{-13}
Mat.1 (Standard)	1.085†	67.12	2.15	1.0013	0.9986	428	300	N/A	0.3497	3.34×10^{-8}
Mat.2 (Standard)	1.085†	67.18	2.15	1.0014	0.9987	432	302	N/A	0.3487	2.80×10^{-8}

†For the standard GSM, we use an end filter with $\alpha_f = 10-2$ at the end of the optimization (end filter). This value was obtained considering the filtered structure solved using Tikhonov regularization. The objective value in the standard GSM for both Materials 1 and 2 before applying the final cutoff is 1.081

material nonlinearity, the members in the optimized structure all have the same value of strain energy density, which corresponds to the full stress design in the linear case, as discussed in Section 2.6. The final topologies, corresponding convergence plots for the objective function, and stress-stretch plots are shown in Fig. 8a, c and e. The normalized cross-sectional areas for the truss members in the final designs are shown in Fig. 8b, d, and f for linear material, Ogden-based materials 1 and 2, respectively.

Table 2 presents a summary of the data associated with Example 1, all the data are obtained after removing aligned nodes. From the CPU run-time comparison, the computational efficiency using the filtering scheme is greater than those without the proposed filter, which shows the advantages of using the filtering technique, particularly for a nonlinear problem. Figure 9 further shows the size reduction history for optimization using Ogden-based Material 2 with the proposed filtering scheme, the numbers of nodes and truss members at optimization steps 50, 150, 250, and 355 (final step) are shown together with the corresponding topologies during the optimization process. The numbers of truss members and nodes in the problem are reduced dramatically by the use of the proposed filtering scheme (with ROM) during the optimization process. For the nonlinear cases, note that the objective values from the proposed filtering scheme are smaller than those without the filtering scheme even though both cases generate identical topologies (for the same material), and from the Max $|\boldsymbol{u}|$ column (maximum value of the absolute displacement), the structures from the proposed filter have less maximum displacement than those with the standard GSM (the maximum displacement for all cases occurs at the loading point). When the proposed filter is applied, it takes into account only the members that appear in the filtered topology at every optimization step. However, for cases of the standard GSM, all the small area members in the nonlinear FEM process are taken into consideration throughout the optimization process; the members with small area, not plotted in the final topology, still support the load and contribute to the stiffness and objective function (total potential energy at the equilibrium configuration) of the structure, and after applying the cut-off, the resulting objective values increase. This observation shows that the proposed filtering scheme addresses the artificial stiffness problem associated with the standard GSM.

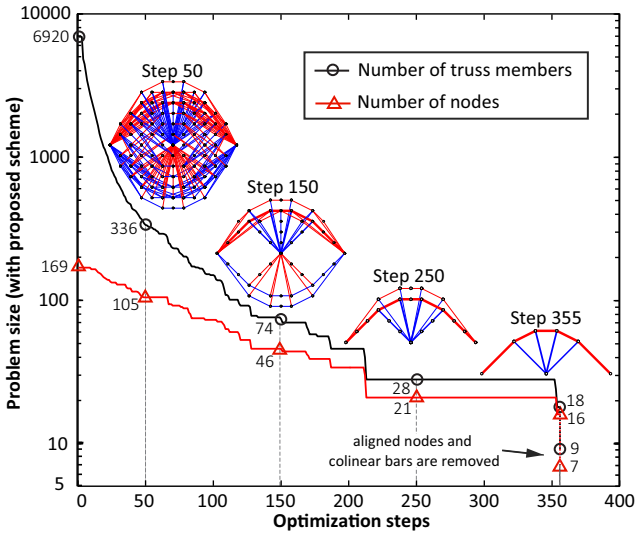

Fig. 9 Size reduction history for optimization using Ogden-based "Material 2" with the proposed filtering scheme. Numbers of truss members and nodes are reduced dramatically by the proposed filtering scheme during the optimization process, which shows the evolution of the ROM

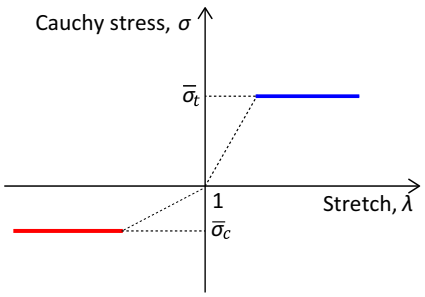

Fig. 10 Stress-stretch diagram for plastic formulation with different stress limits for tension and for compression

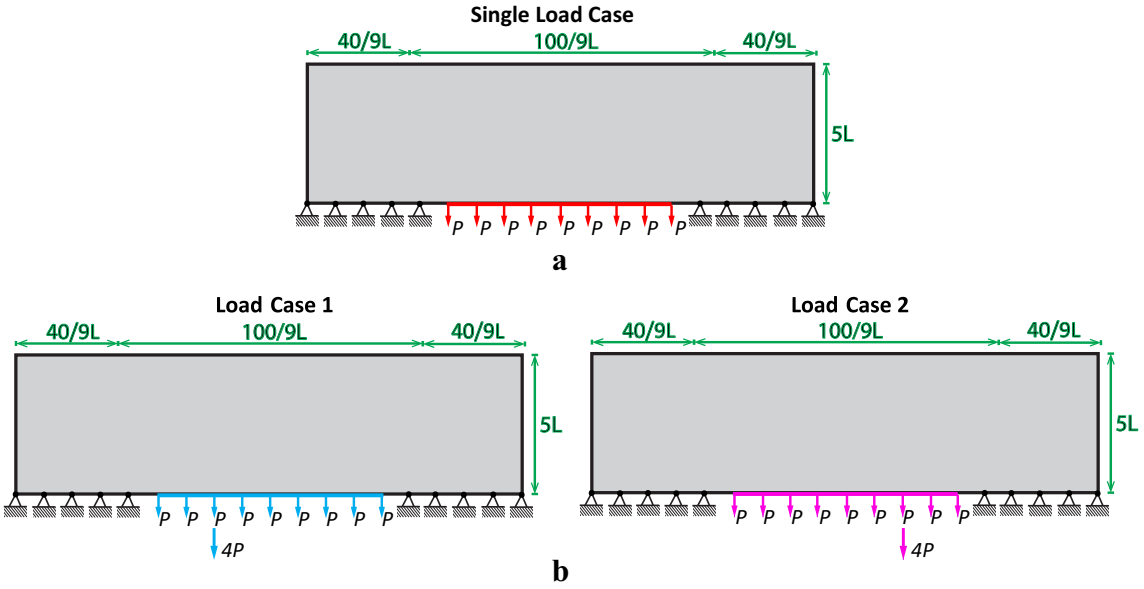

Fig. 11 Two-dimensional bridge domain with a full-level ground structure (18 × 7 grid) and 7,083 non-overlapped bars: geometry ($L = 1m$), load ($P = 40kN$), and support conditions of **a** single load case; **b** multiple load cases

5.2 Example 2: long-span bridge design using bilinear materials

This example shows the influence of different levels of tension and compression of the yield stresses in structural optimization and improvement in the final resolution after using the filter technique. The optimized structures obtained by the proposed algorithm with the single load case and multiple load cases (i.e., the elastic nonlinear formulation with a filter) are then compared with those obtained by the plastic linear formulation with the single load case given in Achtziger (1996). A schematic plot for plastic behavior is shown in Fig. 10. A bridge is modeled using a two-dimensional (2D) domain, shown in Fig. 11a for the single load case and Fig. 11b for the multiple load cases. The domain is discretized by an 18 × 7 grid, followed by the generation of a full-level initial ground structure that contains 7,083 non-overlapping members and 152 nodes. For the multiple load cases, the weighting factor for each load case is the same, i.e., $w_1 = w_2 = 0.5$. To study how an alteration of the tension and compression yield stresses can change the final topology, we use various bilinear materials, each has a unique ratio between the compression and tension Young's moduli, denoted by E_c/E_t. For a linear material with equal tension and compression stress limits, elastic and plastic formulations lead to the same optimized structure up to a rescaling (Hemp 1973; Achtziger 1996). In the case of materials with different tension and compression strengths, the two formulations may not lead to the same solution unless the material properties are defined properly. To compare the results of the elastic nonlinear and plastic linear formulations, the relationship between yield stresses in the plastic formulation and Young's moduli in the elastic formulation is as follows (Achtziger 1996),

$$\frac{\sigma_c}{\sigma_t} = \sqrt{\frac{E_c}{E_t}}. \tag{62}$$

The compression-tension ratios E_c/E_t that we use here are 1, 0.09, 0.04, and 0.0225, shown in Fig. 12, where $E_t = 7 \times 10^7$. In the plastic formulation, the absolute yield stress for tension is fixed, and the absolute yield stress for compression varies from 1 to 0.15. We use a small filter $\alpha_f = 10^{-4}$ throughout the optimization process.

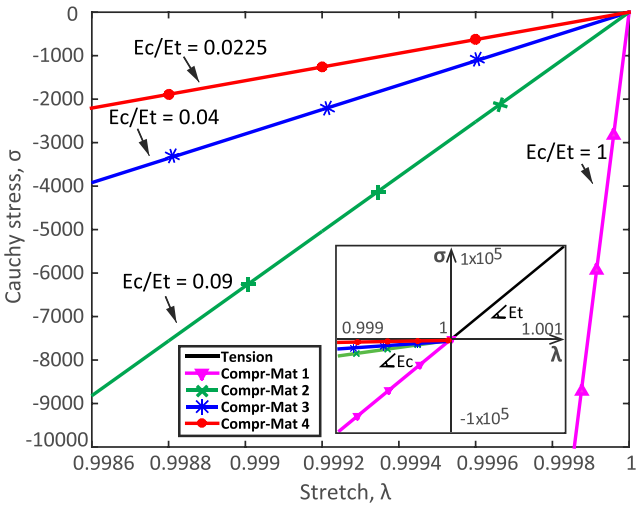

Fig. 12 Bilinear material models. Tension modulus is fixed, and the compression-tension ratios E_c/E_t are 1, 0.09, 0.04, and 0.0225

Figure 13 shows the final topologies of the long-span bridge for the four material models considered. While the top and bottom figures in each sub-figure show the optimized structures from the proposed scheme (i.e., the elastic nonlinear formulation with the filtering scheme for single load case and multiple load cases), those in the middle in each sub-figure show the optimized structures from the plastic linear formulation for single load case by Achtziger (1996). An observation of the final topologies using different ratios of compression-tension strength reveals that the optimized structure transforms from an arch bridge to a suspension bridge. A weaker compression modulus results in fewer bars under compression and more bars under tension. As we decrease the ratio, the arch gradually disappears.

Tables 3 and 4 provide summaries of the numerical information for single load case and multiple load cases in Example 2, respectively. All the data are obtained after removing aligned nodes. Since the tension is fixed and the compression properties vary, a comparison of the final objective values of the different material models indicates the stiffness of each structure differs. When the tension and compression moduli are balanced (Material 1), the final

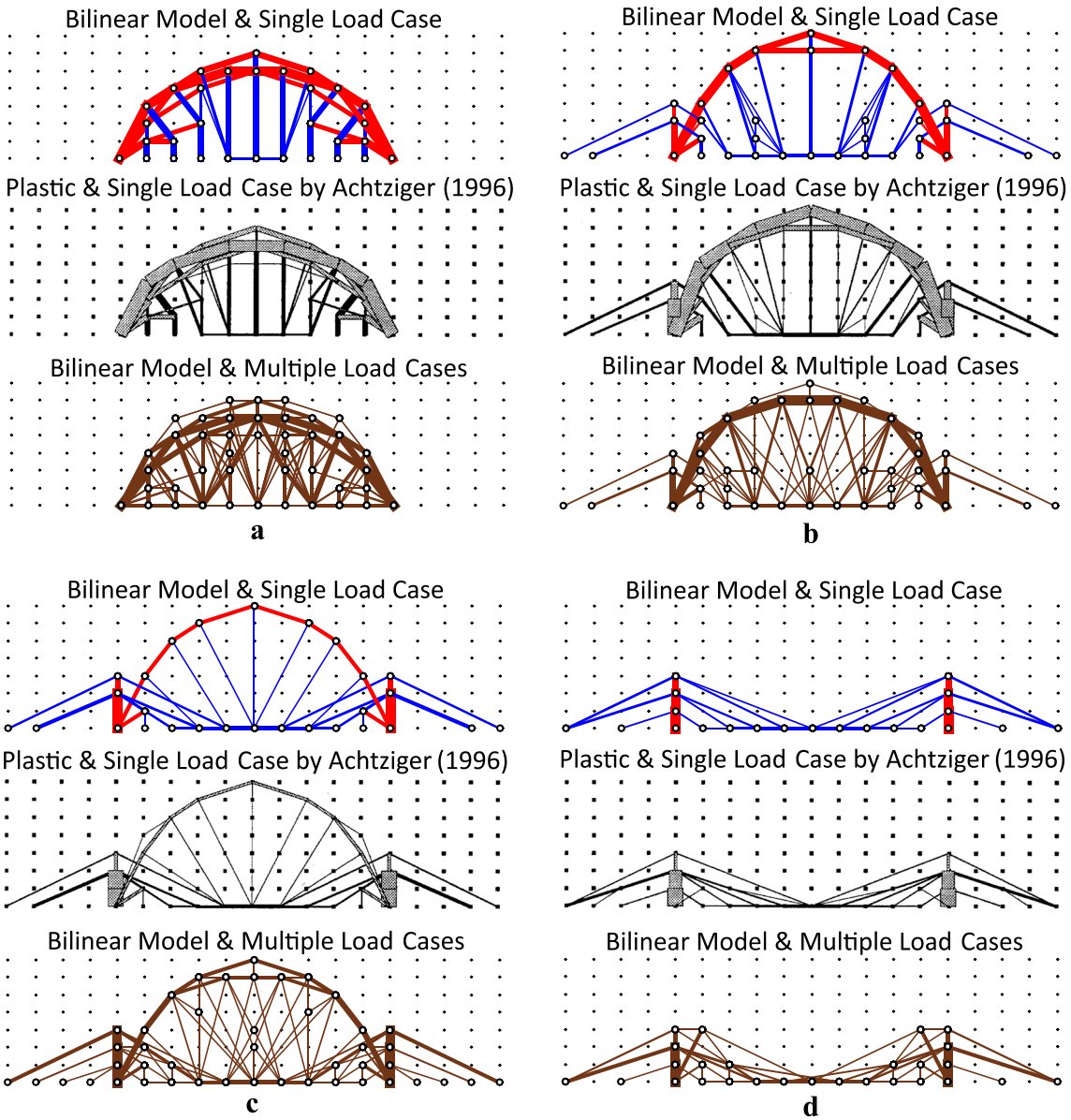

Fig. 13 Optimized structures for **a** "Material 1" with $E_c/E_t = 1$ and $\sigma_c/\sigma_t = 1$; **b** "Material 2" with $E_c/E_t = 0.09$ and $\sigma_c/\sigma_t = 0.3$; **c** "Material 3" with $E_c/E_t = 0.04$ and $\sigma_c/\sigma_t = 0.2$; **d** "Material 4" with $E_c/E_t = 0.0225$ and $\sigma_c/\sigma_t = 0.15$. The *blue bars* are in tension and the *red bars* are under compression. The *brown bars* represent results from multiple load cases (online version in color)

Table 3 Numerical information for the long-span bridge (Example 2) considering the elastic formulation with the proposed filter under single load case

E_t/E_c	$J(\boldsymbol{x}^*)$ (kN · m)	$\Psi(\boldsymbol{u}(\boldsymbol{x}^*))$ (kN/m^2)	Max$\lvert\boldsymbol{u}\rvert$ (cm)	Max λ	Min λ	# Opt. Steps	CPU (sec)	α_f	α_{Top}	$\frac{\lvert\lvert\boldsymbol{R}_{\mathrm{Top}}\rvert\rvert}{\lvert\lvert\boldsymbol{F}_{\mathrm{Top}}\rvert\rvert}$	#Top. Elem.
1	1.92	38.4	1.43	1.0010	0.9990	2,284	49	10^{-4}	0.0165	2.34×10^{-13}	50
0.09	12.25	245.0	8.98	1.0026	0.9912	950	23		0.000382	4.09×10^{-13}	58
0.04	21.96	439.3	18.05	1.0035	0.9823	585	17		0.00657	1.21×10^{-13}	41
0.0225	29.57	591.4	25.85	1.0041	0.9726	272	12		0.0265	1.21×10^{-13}	30

topologies (Fig. 13a) for both the single and multiple load cases have the smallest objective values among all materials, which suggest that those structures have the greatest stiffnesses for this design problem. We confirm this observation by comparing the maximum displacement and strain energy density of all the materials, the topology of Material 1 exhibits the smallest deflection and strain energy density. In contrast, the topology using Material 4 (i.e., Fig. 13d), which has the weakest compressive strength, exhibits the most flexible optimal structures for both single and multiple load cases. Since tension is preferable, the distributed loads must be supported by truss members under tension, forming a suspension bridge in which compression does not appear in the topology except in the supporting two columns. Nevertheless, optimization using Material 4 requires the least amount of computational time. Therefore, the different tension and compression strengths of truss members significantly influence the optimization of a structure.

We further compare the optimized structures from the proposed algorithm (i.e., the elastic nonlinear formulation with a filter) under single load case with those from the plastic linear formulation under single load case used by Achtziger (1996). The comparison shows that the two formulations lead to similar optimal structures for each material and that the proposed filtering scheme improves the resolution of the final topologies and eliminates some of the small area members from the final topology, shown in Fig. 13a, c and d. Comparison between the single and multiple load cases shows that the designs accounting for multiple load cases provide alternative structures, showing the capability of the elastic formulation in accounting for multiple load cases as oppose to the plastic formulation.

5.3 Example 3: top central load on a laterally constrained parallelepiped domain

In this example, we first show the influence of the load level on the resulting topology when both linear and nonlinear materials are taken into account, followed by the demonstration of the computational capability of the proposed method on models with varying number of design variables. We use a small filter $\alpha_f = 10^{-4}$ throughout the optimization process, followed by a larger filter $\alpha_f = 10^{-2}$ in the final step of the optimization to control the resolution of the final topology. After the last filter, we ensure equilibrium of the final structure by checking the global equilibrium. The comparison of different load levels utilizes a coarse discretization with an Ogden-based material and has three imposed load levels (5 kN, 20 kN, and 100 kN). This comparison also includes a linear material with one imposed load level (5 kN) since the linear case is independent of the load level. We use a $14 \times 14 \times 5$ grid for the coarse discretization and generate a level 5 initial ground structure containing 279,653 non-overlapped members. The geometry, the load, and support conditions are shown in Fig. 14a, and the Ogden-based material model with greater strength in tension is shown in Fig. 14b.

Figure 15 shows the optimized topologies for the nonlinear material under three load levels: $P = 5$ kN, $P = 20$ kN, and $P = 100$ kN. Note that Fig. 15a also represents the

Table 4 Numerical information for the long-span bridge (Example 2) considering the elastic formulation with the proposed filter under multiple load cases

E_t/E_c	$J(\boldsymbol{x}^*)$ (kN · m)	$\sum_{j=1}^{2} w_j \Psi(\boldsymbol{u}_j(\boldsymbol{x}^*))$ (kN/m^2)	# Opt. Steps	CPU (sec)	α_f	α_{Top}	$\frac{\lvert\lvert\boldsymbol{R}_{\mathrm{Top}}\rvert\rvert}{\lvert\lvert\boldsymbol{F}_{\mathrm{Top}}\rvert\rvert}$	# Top. Elem.
1	5.40	108.1	6399	216	10^{-4}	0.00111	9.98×10^{-14}	117
0.09	31.28	625.6	2891	116		0.000198	1.08×10^{-13}	94
0.04	56.60	1132.0	1193	66		0.000207	1.18×10^{-13}	96
0.0225	75.77	1515.4	224	32		0.00532	2.26×10^{-13}	52

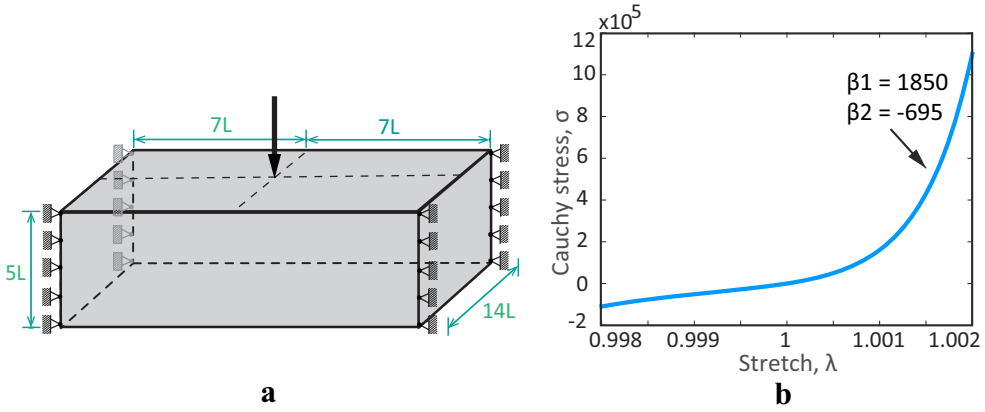

Fig. 14 A laterally constrained rectangular domain with single load case. **a** Problem domain ($L = 1m$), load, and boundary conditions; **b** Ogden material model (tension-dominated)

topology of the linear material case. At the 5kN load, the nonlinear material case yields the same topology as the linear material case. The small differences in their objective and displacement values are due to the minor nonlinearity that exists at this load level in the nonlinear material case. As the load level increases, the topology of the linear model does not change; the corresponding topologies of the nonlinear cases, however, change dramatically. As a consequence of the relatively stiffer tension strength of the chosen material model, a higher load leads to a relatively larger stretch, which results in more truss members under tension than at the lower load levels. This observation shows the importance of accounting for material nonlinearity. In addition, to demonstrate the influence of the line search method, which is described in Section 3.5, we solve the nonlinear model of $P = 100$kN by the Newton-Raphson method with and without the line search method. The nonlinear FEM iterations for first, second, and final optimization steps are shown in Table 5. In the initial optimization step, while the case without the line search method fails to converge, the case with the line search converges within 11 FEM iterations. As a result, the Newton-Raphson method with line search reaches the optimal solution. Table 6 presents a summary of the numerical information for the comparison of different load levels with Max $|\boldsymbol{u}|$ confirming the small displacement assumption used in this work, all the data are obtained after removing aligned nodes.

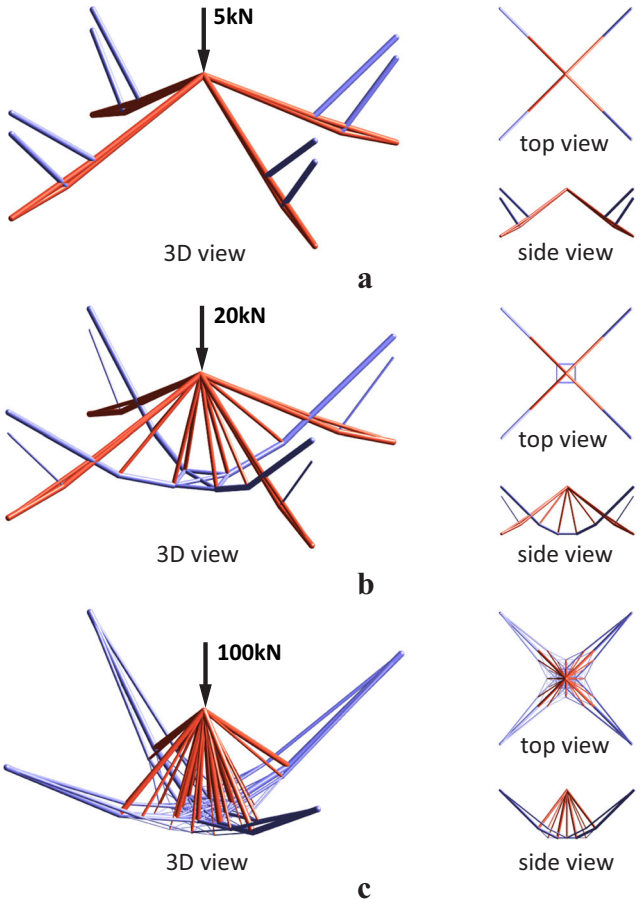

Fig. 15 Final topologies by imposing different load levels in the proposed filtering scheme with a level 5 ground structure ($14 \times 14 \times 5$ grid) and 279,653 non-overlapped bars using **a** Ogden-based material and linear material, each carrying a 5 kN load (these two materials under 5 kN load lead to the same topology); **b** Ogden-based material carrying a 20kN load; and **c** Ogden-based material carrying a 100 kN load (online version in color)

Furthermore, we demonstrate the potential of the filtering scheme in dealing with problems with a relatively large number of design variables by comparing the computational efficiency of the proposed filtering scheme with that of the standard GSM without the proposed filter. For a fair comparison, both approaches (filter and standard GSM) use the same Ogden-based material (Fig. 14b), initial grid ($18 \times 18 \times 6$), connectivity level (level 7), and load level ($P = 1,000$KN), leading to the same initial ground structures with 1,062,090 non-overlapped members and 2,527 nodes. The final topologies for both cases are shown in Fig. 16, and their associated numerical data are recorded in Tables 7 and 8. Using the standard GSM, since numerous small area bars are not plotted on the final topology while still supporting the structure, after the final cut-off,

Table 5 Influence of the line search method for the case $P = 100$kN (Example 3)

Newton-Raphson with line search				Newton-Raphson without line search		
Opt. step	FEM iter.	Step length, ξ	$\frac{\|\|R_{\text{Top}}\|\|}{\|\|F_{\text{Top}}\|\|}$	Opt. step	FEM iter.	$\frac{\|\|R_{\text{Top}}\|\|}{\|\|F_{\text{Top}}\|\|}$
1	1	0.0313	7.408×10^{-1}	Fails to converge		
	2	0.250	1.277			
	3	1.000	9.015			
	4	1.000	3.323			
	5	1.000	1.206			
	⋮	⋮	⋮			
	12	1.000	1.095×10^{-9}			
2	1	1.000	2.778×10^{1}			
	2	1.000	1.000×10^{1}			
	⋮	⋮	⋮			
	9	1.000	1.378×10^{-9}			
522 (Final)	1	1.000	2.800×10^{-5}			
	2	1.000	5.023×10^{-9}			

Table 6 Numerical information for Example 3 (Fig. 14) - influence of the load level considering material nonlinearity. We use $\alpha_f = 10^{-4}$ during the optimization process followed by an end filter with $\alpha_f = 10^{-2}$

	$J(\boldsymbol{x}^*)$ (kN · m)	$\Psi(\boldsymbol{u}(\boldsymbol{x}^*))$ $\left(\text{kN}/m^2\right)$	Max$\|\boldsymbol{u}\|$ (cm)	Max λ	Min λ	# Opt. Steps	CPU (sec)	α_{Top}	Equilibrium Residual	#Top. Elem.
Linear 5kN	0.00724	0.59	0.29	1.0000**	0.9999	3,005	85	1.00	1.64×10^{-8}	24
NonL 5kN	0.00759	0.40	0.31	1.0000**	0.9999	3,005	800	1.00	3.55×10^{-9}	24
NonL 20kN	0.0968	4.87	0.97	1.0004	0.9996	707	634	0.143	8.10×10^{-10}	48
NonL 100kN	1.856	64.42	3.15	1.0010	0.9984	522	582	0.0108	1.42×10^{-9}	132

**The exact maximum stretch value for both linear ($P = 5kN$) and nonlinear ($P = 5kN$) cases is 1.000023

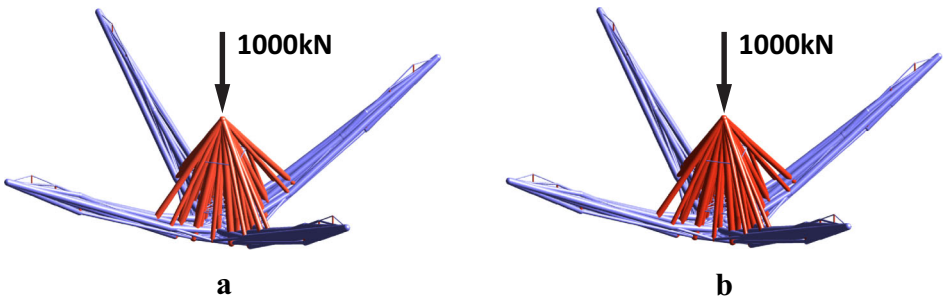

Fig. 16 Results of the optimization for the comparison of the filtering scheme with the standard GSM using a level 7 ground structure (18 × 18 × 6 grid) and 1,062,090 non-overlapped members at a 1,000 kN load level: **a** The final topology obtained from the proposed filtering scheme ($\alpha_f = 10^{-4}$), CPU time 54 minutes; and **b** the final topology (almost identical to the previous one) obtained from the standard GSM, CPU time 40.3 hours

Table 7 Numerical information for Example 3 (Fig. 14) - comparison of filter with standard GSM. For both the filter approach and the standard GSM, we use an end filter with $\alpha_f = 10^{-2}$ at the end of the optimization (end filter)

	$J(\boldsymbol{x}^*)$ $(\text{kN} \cdot m)$	$\Psi(\boldsymbol{u}(\boldsymbol{x}^*))$ (kN/m^2)	Max$\lvert\boldsymbol{u}\rvert$ (cm)	Max λ	Min λ	# Opt. Steps	CPU	α_f	α_{Top}	$\frac{\lvert\lvert R_{\text{Top}}\rvert\rvert}{\lvert\lvert F_{\text{Top}}\rvert\rvert}$	#Top. Elem.
NonL 1000 kN (Filter)	63.53	998	8.41	1.0024	0.9947	962	54 mins	10^{-4}	0.0109	1.30×10^{-13}	425
NonL 1000 kN (Standard)	63.74†	1,001	8.43	1.0024	0.9948	1,050	40.3 hours	N/A	0.0101	3.51×10^{-12}	417††

†This value was obtained considering the filtered structure solved using Tikhonov regularization. The objective value in the standard GSM before applying the final cutoff (end filter) is 63.72

††The number of truss elements in the standard GSM during the entire optimization process is 1,062,090

we observe a larger maximum displacement and a larger objective value.

The proposed filter approach, while offering a nearly identical topology and objective value as the standard GSM, drastically reduces the computational cost. The CPU time used in the optimization process is almost 45 times as fast (54 minutes vs. 40.3 hours), as shown in Table 7, all the data are obtained after removing aligned nodes. As explained previously, the use of the proposed filtering scheme with the ROM reduces the sizes of design variables, the stiffness matrices, and the sensitivity vectors, which significantly decrease the CPU time and memory usage; the standard GSM maintains a constant size during the entire optimization process. To quantify the influence of using the proposed filtering scheme with the reduced-order model on the nonlinear optimization problem, we measure the sizes of the DOFs and design variables at optimization step 1 (initial step), 10, 100, and 962 (final step) during the optimization process for the case with 1000kN load level with the proposed scheme (Fig. 16a). The size reduction history, recorded in Table 8, shows that after performing only 10 steps in the optimization process (962 steps in total), the size of the design variables reduces to nearly 1 % of its original size.

5.4 Example 4: arch bridge

To illustrate the influence that nonlinear materials may have on actual structures, we use a 3D bridge design with three Ogden-based materials. The bridge domain in Fig. 17a and b has simple supports, a non-designable layer that represents the bridge deck, and a void zone for practical design purposes (Zegard and Paulino 2015b). In an effort to obtain constructible structures, we use a $10 \times 6 \times 10$ grid to discretize the domain followed by the generation of a full-level initial ground structure that contains 231,567 non-overlapping members. To represent the effect of the bridge deck, we use a layer of beam elements excluded from the optimization process but included in the nonlinear FEM analysis. To study how any alteration in the material behavior changes the optimized structure, we use three Ogden-based materials, shown in Fig. 17c. Material 1 ($\beta_1 = 1,850$, $\beta_2 = -695$) has higher tensile strength than compressive strength, Material 2 ($\beta_1 = 723$, $\beta_2 = -720$) has the similar tension and compression, and Material 3 ($\beta_1 = 698$, $\beta_2 = -1,845$) is relatively stronger in compression than tension. It should be noted that, in addition to a small filter ($\alpha_f = 10^{-4}$) used in the entire optimization, we use a larger filter ($\alpha_f = 10^{-2}$) in the final step of the optimization to control the resolution of the final topology. We ensure the equilibrium of the final structure with the global equilibrium check. Figure 18 shows the optimized structures obtained using the three materials. A detailed summary of

Table 8 Size reduction history for the proposed filter with reduced-order modeling (NonL, 1000kN & Filter)

Opt. step	DOFs		Design variables	
	Size	% of initial size	Size	% of initial size
# 1 (initial)	7,581	100 %	1,062,090	100 %
# 10	2,457	32.4 %	13,850	1.3 %
# 100	645	8.5 %	1,094	0.1 %
# 962 (final)	303	4 %	437	0.04 %

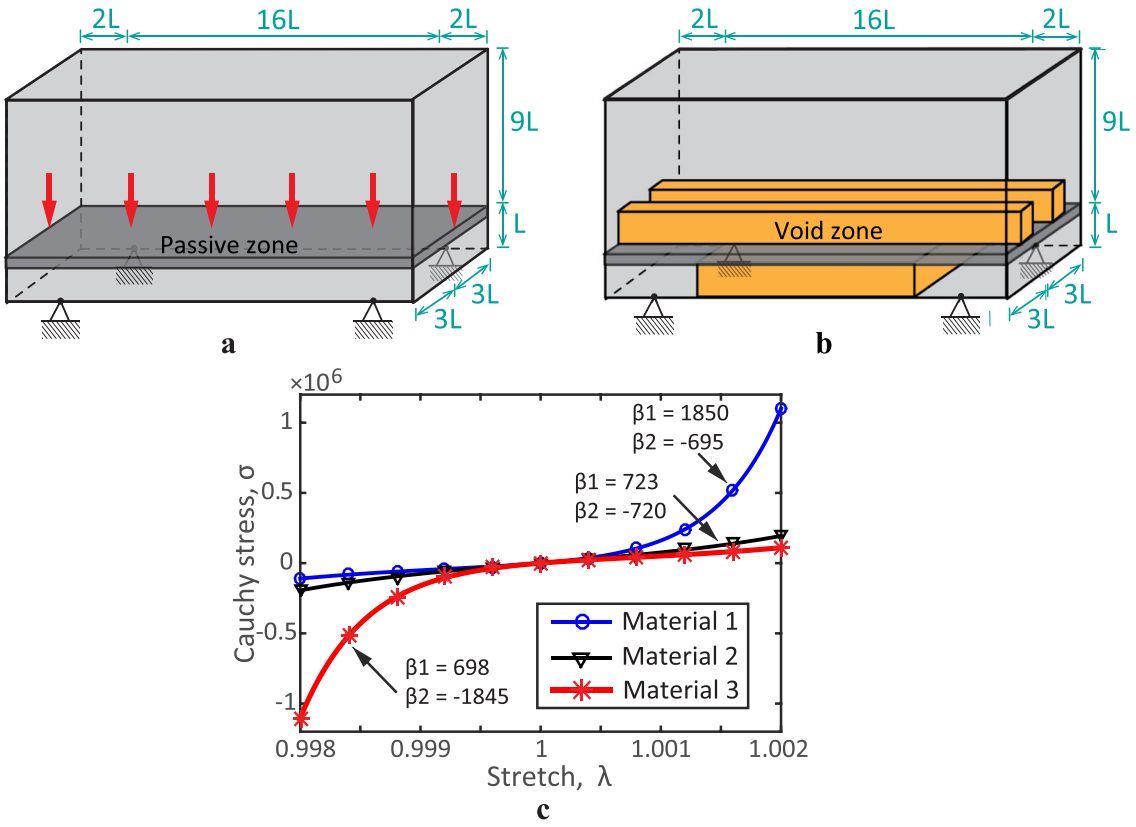

Fig. 17 Three-dimensional bridge design with a level full ground structure ($10 \times 6 \times 10$ grid) and 231,567 non-overlapped members. **a** Design domain ($L = 10m$) with load and boundary conditions; **b** design domain with void zone; **c** Ogden-based material models: "Material 1" has high tensile strength, "Material 2" has a close-to-linear constitutive relationship, and "Material 3" has high compressive strength (online version in color)

the numerical results is provided in Table 9, and all the data are obtained after removing aligned nodes.

The various topologies obtained from using the three materials show the importance of accounting for material nonlinearity. As shown from both Fig. 18 and Table 9, while having only a minor effect on the computational cost of the optimization problem, the choice of material models markedly influences the optimized structures. Optimization using Material 2 with similar compressive and tensional behaviors yields a final topology that resembles an arched bridge, with a significantly larger volume of compression members than of tension members, indicating that the structure requires more compression members because of the nature of the design problem. When Material 1 (with a stronger tension behavior) is used for the design, the overall topology features are similar to those obtained with Material 2, but the final topology contains fewer long compression bars, especially those with small areas in the arch region (because long and thin compression bars result in a large internal energy and, therefore, a large objective), which

Table 9 Numerical information for Example 4 with the proposed reduced-order model. We use $\alpha_f = 10^{-4}$ during optimization process followed by an end filter with $\alpha_f = 10^{-2}$

Material	$J(\boldsymbol{x}^*)$ (kN · m)	$\Psi(\boldsymbol{u}(\boldsymbol{x}^*))$ (kN/m^2)	Max$\lvert\boldsymbol{u}\rvert$ (m)	Max λ	Min λ	Tension Vol.	Compr. Vol.	CPU (sec)	α_{Top}	$\frac{\lvert\lvert\boldsymbol{R}_{\text{Top}}\rvert\rvert}{\lvert\lvert\boldsymbol{F}_{\text{Top}}\rvert\rvert}$
1	370.6	3,934	1.15	1.0030	0.9926	19.8 %	80.2 %	771	0.0474	1.86×10^{-13}
2	394.2	4,742	1.20	1.0066	0.9935	30.4 %	69.6 %	643	0.0115	6.74×10^{-14}
3	259.9	2,773	0.72	1.0074	0.9972	41.0 %	59.0 %	637	0.121	1.06×10^{-13}

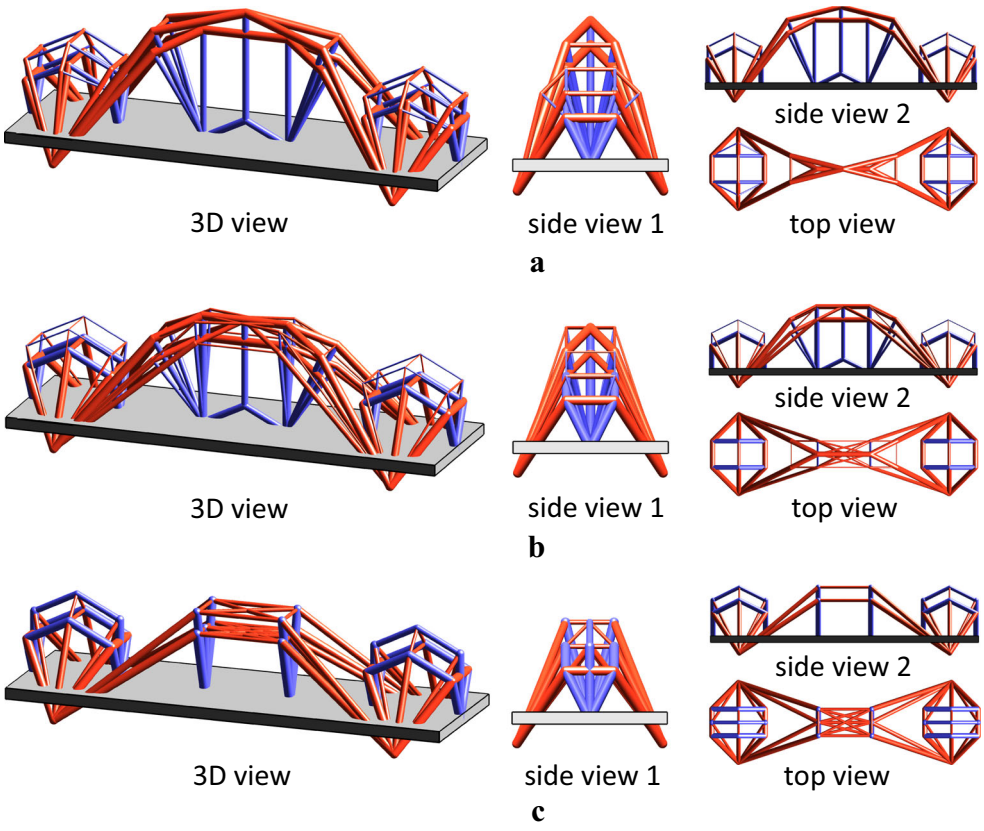

Fig. 18 Final topologies from the proposed filtering scheme using: **a** "Material 1"; **b** "Material 2"; and **c** "Material 3". *Blue* represents bars in tension and *red* represents bars in compression (online version in color)

leads to a clearer topology. We also notice that the total volume of the compression members for Material 1, compared to the one obtained for Material 2, increases and the objective value decreases.

When we use Material 3, with stronger compressive behavior, the final topology shows patterns that differ from those obtained for both Materials 1 and 2, especially in the arch region. The fan area of the arch contains fewer tension members with larger cross-sectional areas that are all connected by long compression members. Indeed, Material 3 exhibits the clearest final topology, as shown by α_{Top} values. Moreover, as a result of the relatively weaker tension behavior, the total volume of the tension bars increases. The objective value is the smallest of the three cases because, as mentioned previously, the structure requires compression members in this problem. A comparison of the heights of the three optimized structures in Fig. 19 shows that higher tensile strength in a material leads to a higher arch in the optimized design. As the tensile strength of the material decreases and compressive strength increases, the height of the arch gradually decreases. The design with Material 3 has the lowest height $5.2L$. The observed differences in the final topologies associated with the three materials with various constitutive relationships demonstrate the importance of accounting for nonlinearity in material models in the practical design optimizations of 3D structures. This example shows that the proposed filtering scheme, which combines the practical demands of material behavior and manufacturing, is a functional design tool. The optimized bridge design with Material 3 (Fig. 18c) is further manufactured by the 3D printing technique using a fused deposition modeling (FDM) process, as shown in Fig. 20. This bridge model is directly manufactured without post-processing of the numerical result.

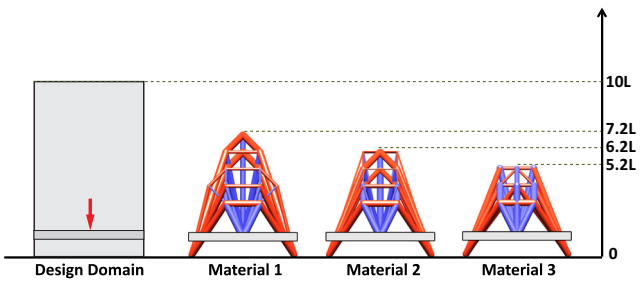

Fig. 19 Comparison of bridge heights for optimized structures using three material models

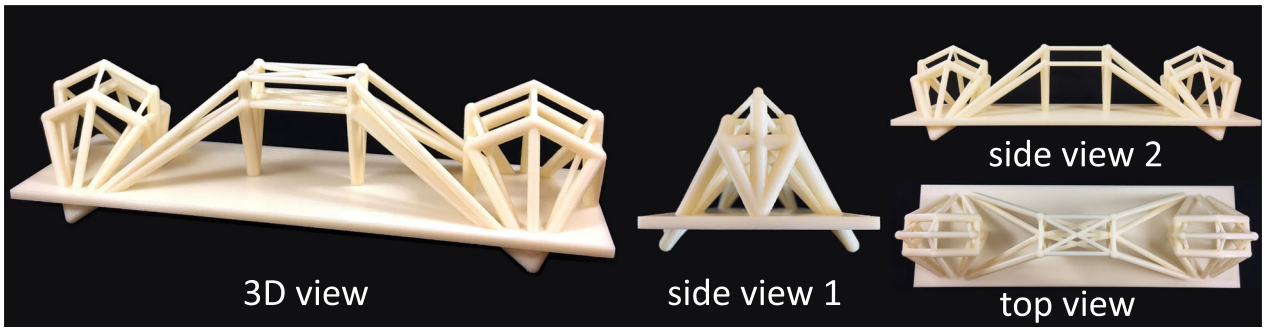

Fig. 20 3D printed model of the optimized bridge design with "Material 3" in Example 4 using a FDM process. The dimension of the manufactured model is 11.5 in × 3.5 in × 3 in

6 Concluding remarks and extensions

This paper proposes an efficient reduced-order discrete filter that can be applied to truss optimization considering single and multiple load cases, and nonlinear constitutive behavior. The proposed scheme utilizes reduced-order modeling on both the state and optimization problems. It examines two types of materials: hyperelastic Ogden-based and bilinear materials, both of which offer alternative options for material behavior. Using a Tikhonov regularization, we solve the singular state equations in the modified standard formulation with design variable $\boldsymbol{x} \geq \boldsymbol{0}$ (see (4)). This modification on the lower bound of design variables transforms the sizing problem (standard formulation) into a topology optimization problem (modified standard formulation). We prove the convexity of the modified standard formulation (4) under the assumptions of convex energy density function and equilibrium satisfaction. This proof is valid even when the tangent stiffness matrix is positive semidefinite. Furthermore, as shown by the KKT conditions (see Section 2.6), our formulation leads to constant weighted sum of specific strain energy under m load cases for those members whose optimal design variables are in the optimum range $0 < x^{(i)^*} < x^{(i)}_{\max}$ (see (19)). An inexact (Armijo-type) line search is adopted in the Newton-Raphson method, which is shown to improve convergence in the first few FEM iterations of the nonlinear structural problem. The line search is essential for convergence.

Based on the present investigation and outcome of the examples, we conclude that the discrete filter with material nonlinearity is a practical tool that accounts for real-life demands of materials, layout, and manufacturing. While traditional topology optimization typically assumes linear material behavior, which may be limiting; we examine material nonlinearity in the optimization that takes into account the effect of proper load levels. Through several examples, we observe the difference in topologies resulting from changes in the material models and load levels, which shows the importance of accounting for nonlinear material behavior in practical design optimization of 2D and 3D structures. In addition, while the optimized structures under single load case obtained from the proposed algorithm (elastic nonlinear formulation with filter) and those from the plastic linear formulation are similar, the designs accounting for multiple load cases provide alternative structures, illustrating the capabilities of the elastic formulation in accounting for multiple load cases and nonlinear behavior.

With the proposed filtering scheme, we solve structural problems solely from information about truss members remaining in the structure. In addition, through comparison with the standard GSM, we conclude that while including the small area members that are below the cut-off (i.e., standard GSM) to solve nonlinear structural problems may result in artificial stiffness and convergence difficulties, excluding them with the Tikhonov regularization technique (with or without the filtering scheme) provides better control in the condition number of the tangent stiffness matrix. Moreover, because we can use the proposed filter to control the final resolution of the optimized structure, the results may be manufactured without post-processing (see Fig. 20).

The use of the (fully) reduced-order modeling in the proposed filtering scheme significantly reduces the size of both the structural and optimization problems within a few optimization steps, leading to drastically improved computational performance. Through one study conducted in this paper (see Section 5.3), the proposed filter algorithm, while offering almost the same optimized structure, was 45 times faster than the standard GSM for nonlinear optimization problems.

The proposed regularization technique to solve nonlinear problems can be combined with other types of filters, for instance, only applying an end filter at the end of the optimization process, or applying the filter at different intervals, i.e., $N_f \geq 1$, instead of applying at every optimization

step. This work provides several directions for future research, including applying the proposed filtering scheme to multi-material optimization and additive manufacturing (Zegard and Paulino 2015a), optimization accounting for geometric nonlinearity, and combining this technique (the filtering scheme with discrete optimization) with the continuum optimization (density-based) method.

Acknowledgments The authors acknowledge the financial support from the US National Science Foundation (NSF) under projects #1559594 (formerly #1335160) and #1321661, from the Brazilian agency CNPq (National Council for Research and Development), and from the Laboratory of Scientific Computing andVisualization (LCCV) at the Federal University of Alagoas (UFAL). We are also grateful for the endowment provided by the Raymond Allen Jones Chair at the Georgia Institute of Technology. The information provided in this paper is the sole opinion of the authors and does not necessarily reflect the views of the sponsoring agencies.

Appendix A: filter function

```
%--------------------------- Filter Function -----------------------------%
% Ref: X Zhang, AS Ramos Jr., GH Paulino, "A Discrete Filter Scheme for   %
% Material Nonlinear Topology Optimization Using the Ground Structure     %
% Method".                                                                %
%-------------------------------------------------------------------------%
%% An example of the filter for a randomly generated vector
n=20; % Size of the random vector
alpha_f=0.4; % Filter value
xr=rand(n,1)*10; % Generate the random vector
%% ---------------------------------------------------------------------
% Option 1: Perform filter component-wise (see Eq. 6)
xr_f=zeros(n,1);
for i=1:n
    if xr(i)/max(xr)<alpha_f
        xr_f(i)=0;
    else
        xr_f(i)=xr(i);
    end
end
%% ---------------------------------------------------------------------
% Option 2: Perform filter for the entire vector
% xr_f=xr;
% xr_f(xr/max(xr)<alpha_f)=0;
%% ---------------------------------------------------------------------
figure
plot(xr/max(xr),xr_f,'ro')
xlabel('x_r^{(i)}/max(x_r)');ylabel('Filter(x_r,\alpha_f,i)');
% Filtered vector with reduced-order modeling
xr_f=xr_f(xr_f>0);
```

Appendix B: Mapping for the state equations using the proposed filtering scheme with reduced-order modeling

Based on the equations outlined in Section 4.1, this section illustrates the mapping of the external and internal force vectors and the tangent stiffness matrix from the ground structure to the topology through a simple example. Figure 21a shows the ground structure with numbered DOFs under the prescribed load and boundary conditions. During the optimization process, once the members are removed by the filter, area of members become zero , (e.g., the dashed

members in Fig. 21b), we can define the topology and new numbered DOFs by excluding those zero-area members, as shown in Fig. 21c.

For the ground structure, the external force vector are given by,

$$\{\boldsymbol{F} = 0 \quad 0 \quad -P \quad 0 \quad 0 \quad \}^{\mathrm{T}}. \tag{63}$$

The internal force vector and tangent stiffness matrix are obtained by assembling the contributions from each element,

$$\boldsymbol{T} = \begin{Bmatrix} t_1^{(1)} + t_1^{(2)} \\ t_2^{(2)} + t_2^{(3)} + t_2^{(5)} \\ t_3^{(2)} + t_3^{(3)} + t_3^{(5)} \\ t_4^{(4)} + t_4^{(5)} \\ t_5^{(4)} + t_5^{(5)} \end{Bmatrix}, \tag{64}$$

$$\boldsymbol{K}_t = \begin{bmatrix} k_{11}^{(1)} + k_{11}^{(2)} & k_{12}^{(2)} & k_{13}^{(2)} & 0 & 0 \\ & k_{22}^{(2)} + k_{22}^{(3)} + k_{22}^{(5)} & k_{23}^{(2)} + k_{23}^{(3)} + k_{23}^{(5)} & k_{24}^{(5)} & k_{25}^{(5)} \\ & & k_{33}^{(2)} + k_{33}^{(3)} + k_{33}^{(5)} & k_{34}^{(5)} & k_{35}^{(5)} \\ & \text{Sym.} & & k_{44}^{(4)} + k_{44}^{(5)} & k_{45}^{(4)} + k_{45}^{(5)} \\ & & & & k_{55}^{(4)} + k_{55}^{(5)} \end{bmatrix}. \tag{65}$$

We can define a transformation matrix $\boldsymbol{Q}$ to represent the transformation of the topology displacements to the ground structural displacements (i.e., $\boldsymbol{u} = \boldsymbol{Q}\boldsymbol{u}_{\mathrm{Top}}$),

$$\boldsymbol{Q} = \begin{bmatrix} 1 & 0 & 0 & 0 & 0 \\ 0 & 1 & 0 & 0 & 0 \\ 0 & 0 & 1 & 0 & 0 \end{bmatrix}^{\mathrm{T}}. \tag{66}$$

With the transformation matrix, the external force vector for the reduced-order topology is given by

$$\boldsymbol{F}_{\mathrm{Top}} = \boldsymbol{Q}^{\mathrm{T}}\boldsymbol{F} = \{ 0 \quad 0 \quad -P \}^{\mathrm{T}}. \tag{67}$$

Similarly, the internal force vector and tangent stiffness matrix for the reduced-order topology can be obtained as follows:

$$\boldsymbol{T}_{\mathrm{Top}} = \boldsymbol{Q}^{\mathrm{T}}\boldsymbol{T} = \begin{Bmatrix} t_1^{(1)} + t_1^{(2)} \\ t_2^{(2)} + t_2^{(3)} + t_2^{(5)} \\ t_3^{(2)} + t_3^{(3)} + t_3^{(5)} \end{Bmatrix}, \tag{68}$$

$$\boldsymbol{K}_{t,\mathrm{Top}} = \boldsymbol{Q}^{\mathrm{T}}\boldsymbol{K}_t\boldsymbol{Q} = \begin{bmatrix} k_{11}^{(1)} + k_{11}^{(2)} & k_{12}^{(2)} & k_{13}^{(2)} \\ & k_{22}^{(2)} + k_{22}^{(3)} + k_{22}^{(5)} & k_{23}^{(2)} + k_{23}^{(3)} + k_{23}^{(5)} \\ & \text{Sym.} & k_{33}^{(2)} + k_{33}^{(3)} + k_{33}^{(5)} \end{bmatrix}. \tag{69}$$

Upon realizing that member 5 is a zero-area member, all the components of its internal force vector and tangent stiffness matrix are zero. As s result, we obtain the final expression for the internal force vector and tangent stiffness matrix for the reduced-order topology as

$$\boldsymbol{T}_{\mathrm{Top}} = \begin{Bmatrix} t_1^{(1)} + t_1^{(2)} \\ t_2^{(2)} + t_2^{(3)} \\ t_3^{(2)} + t_3^{(3)} \end{Bmatrix},$$

$$\boldsymbol{K}_{t,\mathrm{Top}} = \begin{bmatrix} k_{11}^{(1)} + k_{11}^{(2)} & k_{12}^{(2)} & k_{13}^{(2)} \\ & k_{22}^{(2)} + k_{22}^{(3)} & k_{23}^{(2)} + k_{23}^{(3)} \\ & \text{Sym.} & k_{33}^{(2)} + k_{33}^{(3)} \end{bmatrix}. \tag{70}$$

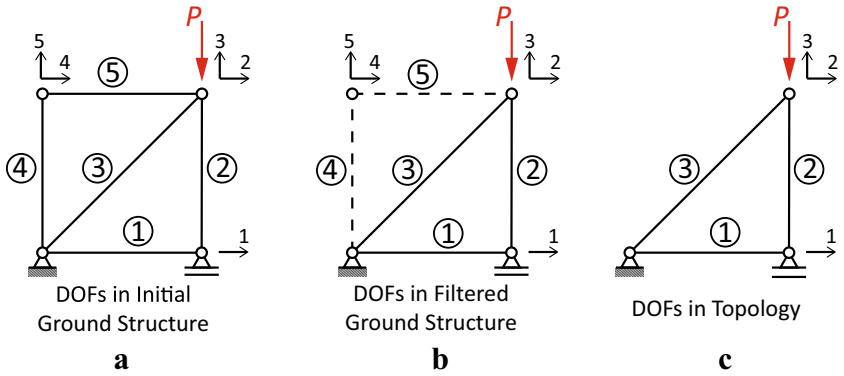

Fig. 21 Mapping of the state equations from the ground structure to the topology with the proposed filtering scheme: **a** Initial ground structure, DOFs, load and boundary conditions; **b** ground structure and DOFs after the filtering process at iteration k (*dashed lines* correspond to bars with zero cross-sectional area); **c** corresponding topology and DOFs after filtering process at iteration k

Appendix C: Nomenclature

α_{Top}	Resolution of the structural topology
α_f	Filter value
ξ^k	Step length at iteration k in the line search scheme
η, η_0	Tikhonov regularization parameters
γ_i, β_i	Ogden material parameters
κ	Scale parameter of the step length in line search
λ	Linearized stretch
Λ, μ	Lamé constants
λ_i	Principal stretches
Ω	Potential energy of external loads
Π	Total potential energy
Ψ	Strain energy density function
Ψ_{Bi}	Bilinear strain energy density function
Ψ_{OG}	Ogden strain energy density function
ρ	Global equilibrium tolerance in nonlinear FEM
σ_c	Reference Cauchy stress in compression
σ_{ij}	Components of the Cauchy stress tensor
σ_t	Reference Cauchy stress in tension
τ	Guard constant in the line search scheme
$\boldsymbol{B}^{(i)}$	Unit directional vector in global coordinates of member i
$\boldsymbol{F}$	External force vector
$\boldsymbol{F}_{\text{Top}}$	External force vector in the structural topology defined by the filter
$\boldsymbol{K}_t$	Global tangent stiffness matrix
$\boldsymbol{K}_t^{(i)}$	Tangent stiffness matrix for member i in global coordinates
$\boldsymbol{k}_t^{(i)}$	Tangent stiffness matrix for member i in local coordinates
$\boldsymbol{K}_{t,\text{Top}}$	Global tangent stiffness matrix for structural topology defined by filter
$\boldsymbol{L}$	Truss member length vector
$\boldsymbol{R}$	Residual force vector
$\boldsymbol{T}$	Internal force vector
$\boldsymbol{t}^{(i)}$	Internal force vector in local coordinates for member i
$\boldsymbol{u}$	Displacement vector
$\boldsymbol{u}^{(i)}$	Displacement vector for member i
$\boldsymbol{u}_j$	Equilibrating displacement vector for load case $\boldsymbol{F}_j$
$\boldsymbol{u}_{\text{Top}}$	Displacement vector in structural topology defined by the filter
$\boldsymbol{u}_p$, $\boldsymbol{u}_q$	Displacements of nodes p and q
$\boldsymbol{x}_f$	Filtered subset of the design variables
d	Number of dimensions
E_0	Initial tangent modulus (Young's modulus)
E_T	Tangent modulus
g	Volume constraint
J	Objective function
$L^{(i)}$	Length of truss member i
M	Ogden material parameter
m	Number of load cases
N	Number of degrees of freedom
n	Number of truss members
$\boldsymbol{N}^{(i)}$	Unit directional vector for member i
N_f	Specified frequency of applying the discrete filter
tol	Tolerance value
U	Internal energy
U_c	Complementary energy at the equilibrium configuration
$V^{(i)}$	Volume of member i
$V_{\max}$	Prescribed maximum volume
$x^{(i)}$	Cross-sectional area of member i (ith design variable)
$x_f^{(i)}$	Filtered cross-sectional area of member i
$x_{\min}^{(i)}$, $x_{\max}^{(i)}$	Lower and upper bounds for the cross-sectional area of member i

References

Achtziger W (1996) Truss topology optimization including bar properties different for tension and compression. Structural Optimization 12(1):63–74

Achtziger W (1997) Topology optimization of discrete structures. Springer, Vienna, pp 57–100

Achtziger W (1999a) Local stability of trusses in the context of topology optimization part I: exact modelling. Struct Multidiscip Optim 17(4):235–246

Achtziger W (1999b) Local stability of trusses in the context of topology optimization part II: a numerical approach. Structural Optimization 17(4):247–258

Armijo L (1966) Minimization of functions having Lipschitz continuous first partial derivatives. Pac J Math 16(1):1–3

Ascher U, Greif C (2011) A first course on numerical methods, vol 7. Society for Industrial and Applied Mathematics

Bendsøe MP, Sigmund O (2003) Topology optimization: theory, methods, and applications. Springer, Berlin

Bertsekas DP (1999) Nonlinear programming. Belmont, Athena Scientific

Bonet J, Wood RD (2008) Nonlinear continuum mechanics for finite element analysis. Cambridge University Press

Bruns T (2006) Zero density lower bounds in topology optimization. Comput Methods Appl Mech Eng 196(1):566–578

Buhl T, Pedersen C, Sigmund O (2000) Stiffness design of geometrically nonlinear structures using topology optimization. Struct Multidiscip Optim 19(2):93–104

Christensen P, Klarbring A (2009) An introduction to structural optimization, vol 153. Springer Science & Business Media, Linköping

Dorn WS, Gomory RE, Greenberg HJ (1964) Automatic design of optimal structures. Journal de Mecanique 3:25–52

Felippa C (n.d) Newton method: general control and variants. Lecture notes. http://www.colorado.edu/engineering/cas/courses.d/NFEM.d/NFEM.Ch26.d/NFEM.Ch26.pdf

Groenwold AA, Etman L (2008) On the equivalence of optimality criterion and sequential approximate optimization methods in the classical topology layout problem. Int J Numer Methods Eng 73(3):297–316

Haftka R, Kamat M (1989) Simultaneous nonlinear structural analysis and design. Comput Mech 4(6):409–416

Hassani B, Hinton E (1998) A review of homogenization and topology optimization iii—topology optimization using optimality criteria. Comput Struct 69(6):739–756

Hemp WS (1973) Optimum structures. Clarendon Press

Kemmler R, Lipka A, Ramm E (2005) Large deformations and stability in topology optimization. Struct Multidiscip Optim 30(6):459–476

Khot N, Kamat M (1985) Minimum weight design of truss structures with geometric nonlinear behavior. AIAA J 23(1):139–144

Kirsch U (1989) Optimal topologies of truss structures. Comput Methods Appl Mech Eng 72(1):15–28

Klarbring A, Rönnqvist M (1995) Nested approach to structural optimization in nonsmooth mechanics. Structural Optimization 10(2):79–86

Klarbring A, Strömberg N (2012) A note on the min-max formulation of stiffness optimization including non-zero prescribed displacements. Struct Multidiscip Optim 45(1):147–149

Klarbring A, Strömberg N (2013) Topology optimization of hyperelastic bodies including non-zero prescribed displacements. Struct Multidiscip Optim 47(1):37–48

Ogden RW (1984) Non-linear elastic deformations. Dover Publications Inc, Mineola

Ohsaki M (2010) Optimization of finite dimensional structures. CRC Press, Boca Raton

Ramos Jr AS, Paulino GH (2015) Convex topology optimization for hyperelastic trusses based on the ground-structure approach. Struct Multidiscip Optim 51(2):287–304

Ramos Jr AS, Paulino GH (2016) Filtering structures out of ground structures – a discrete filtering tool for structural design optimization. Struct Multidiscip Optim 54(1):95–116

Rockafellar R (1970) Convex analysis. Princeton University Press, Princeton

Rozvany GIN, Bendsoe MP, Kirsch U (1995) Layout optimization of structures. Appl Mech Rev 48(2):41–119

Sekimoto T, Noguchi H (2001) Homologous topology optimization in large displacement and buckling problems. JSME Int J Ser A 44:616–622

Sokół T (2011) A 99 line code for discretized Michell truss optimization written in mathematica. Struct Multidiscip Optim 43(2):181–190

Stolpe M (2016) Truss optimization with discrete design variables: a critical review. Struct Multidiscip Optim 53:349–374

Stolpe M, Svanberg K (2001) An alternative interpolation scheme for minimum compliance topology optimization. Struct Multidiscip Optim 22(2):116–124

Stricklin JA, Haisler WE (1977) Formulations and solution procedures for nonlinear structural analysis. Comput Struct 7(1):125–136

Svanberg K (1984) On local and global minima in structural optimization. In: Gallhager E, Ragsdell RH, Zienkiewicz OC (eds) New directions in optimum structural design. Wiley, Chichester, pp 327–341

Svanberg K (1987) The method of moving asymptotes- a new method for structural optimization. Int J Numer Methods Eng 24(2):359–373

Talischi C, Paulino GH (2013) An operator splitting algorithm for Tikhonov-regularized topology optimization. Comput Methods Appl Mech Eng 253:599–608

Tangaramvong S, Tin-Loi F, Gao W (2014) Optimal retrofit of moment resisting frames using braces accounting for geometric nonlinearity and serviceability conditions. Eng Struct 80:189–199

Tikhonov A, Arsenin V (1977) Methods for solving ill-posed problems. Wiley, New York

Toklu Y (2004) Nonlinear analysis of trusses through energy minimization. Comput Struct 82(20):1581–1589

Wang S, de Sturler E, Paulino GH (2007) Large-scale topology optimization using preconditioned Krylov subspace methods with recycling. Int J Numer Methods Eng 69(12):2441–2468

Washizawa T, Asai A, Yoshikawa N (2004) A new approach for solving singular systems in topology optimization using Krylov subspace methods. Struct Multidiscip Optim 28(5):330–339

Wriggers P (2008) Nonlinear finite element methods. Springer Science & Business Media

Zegard T, Paulino GH (2014) GRAND – ground structure based topology optimization for arbitrary 2D domains using MATLAB. Struct Multidiscip Optim 50(5):861–882

Zegard T, Paulino GH (2015a) Bridging topology optimization and additive manufacturing. Struct Multidiscip Optim 53(1):175–192

Zegard T, Paulino GH (2015b) GRAND3 – ground structure based topology optimization for arbitrary 3D domains using MATLAB. Struct Multidiscip Optim 52(6):1161–1184